ORIGINAL PAPER



Timescale of evolution of a late archean collision zone from Coorg, S. India: constraints from zircon and garnet geochronology

Sampriti Basak^{1,9} · Aitor Cambeses² · Sumit Chakraborty¹ · Axel Gerdes^{3,4} · Carsten Münker⁵ · Ina Martinet⁶ · Somnath Dasgupta⁷ · Santanu Kumar Bhowmik⁸

Received: 24 July 2024 / Accepted: 26 August 2025 / Published online: 30 September 2025 © The Author(s) 2025

Abstract

Petrology, geochemistry and geochronology of a metapelite (sillimanite-garnet-biotite-plagioclase-quartz) from the vicinity of the Archean Mercara Shear Zone in Coorg, S. India show that metamorphism at temperatures>850 °C occurred between 2700–3300 Ma (Phase equilibria, thermobarometry, U-Pb dating of zircons and Lu-Hf dating of garnets). Subsequently, the rocks experienced thermal events at lower temperatures at 2400-2600 Ma as well as at 600-640 Ma (U-Pb dates from rutile). There are indications of multiple episodes of metasomatic/ (high temperature) hydrothermal activity during the Archean events. Residence of the rocks at lower temperatures between the high temperature events is indicated by the kinetics of dissolution of zircon in melt. Taken together, this history shows that (a) P-T-t evolution in this Archean collisional setting happened along an overall clockwise path but not in a single continuous loop - episodes at high temperatures were interspersed with residence at cooler temperatures in between, (b) subtle effects of metamorphism that occurred at temperatures below the peak temperature could help to resolve some controversies related to tectonothermal reconstructions in the region (e.g. whether signatures of both - amalgamation of Dharwar and Coorg cratons and activity along an equivalent of the Betsimisaraka suture zone in east-central Madagascar may be present in the region), and (c) the duration of high-temperature events (several 100 million years at ~800 °C) are consistent with an early Earth peel-back style of plate tectonics, rather than modern day plate tectonics, operating in the region at the time.

Keywords Archean metamorphism · Zircon · Garnet · Trace elements · Geochronology · Timescales · Coorg Block · India

Communicated by Daniella Rubatto.

- ⊠ Sampriti Basak sampriti@snm.ku.dk
- ¹ Institute of Geology, Mineralogy and Geophysics, Ruhr-Universität Bochum, 44801 Bochum, Germany
- Department of Mineralogy and Petrology, University of Granada, Granada 18002, Spain
- Department of Geosciences, Goethe-University Frankfurt, 60438 Frankfurt, Germany
- Frankfurt Isotope and Element Research Center (FIERCE), Goethe- University Frankfurt, 60438 Frankfurt, Germany

- Institute of Geology and Mineralogy, University of Cologne, 50674 Cologne, Germany
- ⁶ 50969 Cologne, Germany
- Geological Studies Unit, Indian Statistical Institute, Kolkata, Kolkata 700106, India
- Department of Geology and Geophysics, Indian Institute of Technology, Kharagpur 721302, India
- Present address: Natural History Museum of Denmark, Copenhagen 1350, Denmark



Introduction

Continents on the present-day Earth have multiple cratonic nuclei, which are connected along zones of deformation and metamorphism that are often described by the neutral term "mobile belts". In the present-day plate tectonic regime continents amalgamate along collision zones such as the Himalaya. However, understanding the process of such amalgamation in the Archean requires answers to several questions: (i) Was plate tectonics operative? If not, what was the process of amalgamation? (ii) If plate tectonics was operative, was the style, dynamics, and temporal evolution on a hotter Earth the same as that observed today? (iii) Is deformation and metamorphism in such zones a single stage continuous process, or are such zones the sites of repeated, pulsed events spread over geological time? The record preserved in supracrustal rocks that have been buried, deformed, metamorphosed, and exposed on the surface today provides a means of addressing some of these issues (Van Kranendonk et al. 2018; Cawood et al. 2022).

The Coorg Block in S. India is connected to the Archean Dharwar craton along the Mercara Shear zone (Santosh et al. 2014; Amaldev et al. 2016; Basak et al. 2023). Within this zone, a particular exposure of a metapelitic rock that is also intimately associated with a metabasic lithology preserves multiple stages of metamorphic history, including partial melting. We have used time information from zircon, garnet as well as rutile geochronology and kinetics of zircon dissolution combined with P-T path modelling constrained by metamorphic reaction textures to constrain the temporal evolution and nature of dynamics in this zone of amalgamation (we intentionally avoid the term "suturing" because that term has very specific tectonic connotations in the presentday plate tectonic context). The rocks of this exposure have also been studied by Amaldev et al. (2016) and we use data from their study as well as ours to reach our conclusions.

We use the following nomenclature in this study in order to be able to refer to specific features/processes: We refer to each pressure, temperature, time etc. read from an observational feature (composition, texture interpreted to show a reaction, isotope ratio) as an "event" (i.e. one point in P-T-t coordinate space). These are given sequential names (e.g. M1, M2, ...). Specifically, we do not use the term here in the sense of a metamorphic event (as in "Variscan" event). This distinction is essential for our work because we demonstrate how two successive events may not/need not be connected by a straight-line segment of a P-T path, and the same P-T coordinate may be approached from different directions at different times (i.e. P-T-t coordinates are different) during the evolution of the lithological packet - this is the essence of identifying a pulsed history, with its important tectonic implications.

Geological setting and field relations

The Coorg Block is situated in the southwestern part of Peninsular India. The E-W trending Mercara Shear zone in the north and the WNW-ESE trending Moyar Shear zone in the south bound it. It is an exotic microcontinent that had its evolutionary history distinct from the adjacent terrane of the Dharwar craton (Santosh et al. 2014). The block is dominantly composed of felsic bodies of orthopyroxene bearing granitoids and pyroxene granulites, with individual exposures of garnetiferous mafic granulites close to the proximity of the northerly bounded Mercara shear zones (Fig. 1a). This shear zone is underplated by high density gravity material in the lower crust, as shown by steep gravity gradients (Sunil et al. 2010). Here we report a detailed study of a garnetiferous sillimanite bearing metapelite sequence, located in the Mercara Shear Zone (12°27'25.2" N 75°38'006" E). One of the interesting features of the studied outcrop is the presence of a separate leucocratic domain (referred to as leucosome in the following sample CM27B-17, Fig. 1b) associated with the sillimanite-garnet bearing rock (sample CM 27C-17, Fig. 1c). These leucosomes have homogenously distributed millimeter to centimeter scale garnets. The pelitic lithology is intercalated with mafic rocks in the same exposure but a strong overgrowth prevents a clear contact relationship between the two from being established. The mafic rock consists of orthopyroxene, clinopyroxene and plagioclase and has several leucocratic veins cutting across it (Fig. 1d and e) (Basak et al. 2023). These rocks show presence of garnets at the contact of those leucocratic veins with the host rock. The pelitic rock, however, is devoid of these veins.

Methods

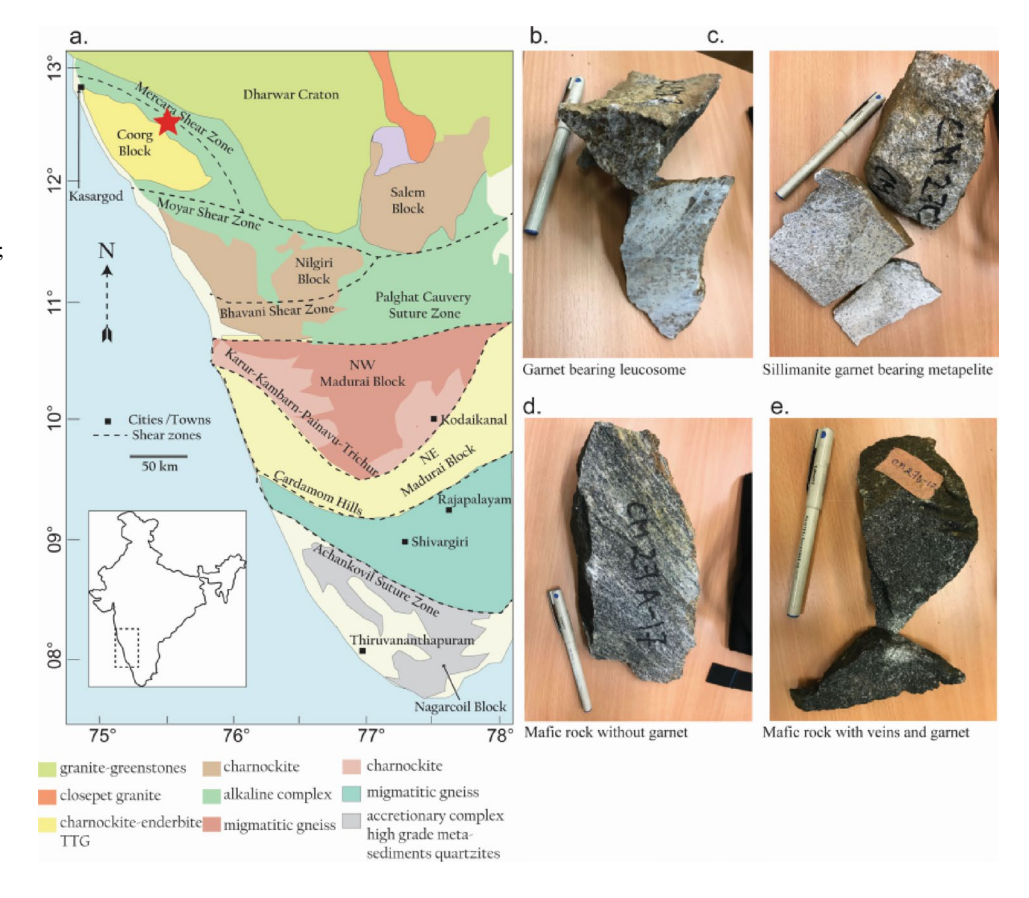
Detailed analytical results on standards for each type of analysis are presented in Supplementary Information Table.

X-Ray fluoresence spectroscopy

Ten major and 29 trace elements were analysed in the laboratory of the Institute of Geology, Mineralogy and Geophysics (GMG), Ruhr University Bochum (RUB). A wavelength dispersive X-Ray spectrometer PHILIPS PW 2401 equipped with a Rh tube was used for the analyses. Conditions for measurement were: 30–52 kV, 40–100 mA for major elements and 32–53 kV, 60–100 mA for trace elements. Regression analysis was done using a de Jong model and 94 certified rock standards were used to obtain calibration curves. The instrument was calibrated using a river sediment (SdAR-1), tonalite (TLM-1) and basalt (BE-N) for



Fig. 1 a Geological map of the Coorg Block redrawn after Chetty et al. (2012), showing the sample location (red star); b Hand specimen picture of the leucosome; c Handspecimen of the sillimanite garnet bearing metapelite; d Handspecimen picture of the adjacent mafic rock without garnet; e Handspecimen of adjacent mafic rock with veins cutting through it and garnet



major element and granitic, (G-2) a basaltic (MBL-1) and a peridotitic (OPY-1) sample for trace element before data acquisition. Analytical results are provided in Supplementary Information Table 1 and normalized trace element plots are shown in Supplementary Material Fig. 1.

Electron probe microanalyses

Minerals such as garnet, plagioclase and biotite were analysed for their major element oxides using a CAMECA SX5 electron microprobe facility enabled with Field Emission Gun (FEG) technique at GMG, RUB. The conditions for measurement of garnets were 15 kV acceleration potential and 20 nA probe current with a Beam diameter was 1 µm. For analyses of plagioclases and micas, a defocused Beam was used with 10-15 nA probe current and a Beam spot size of 5 μm. Standards used for calibration were Si-Olivine (San Carlos-233), Ti-Synthetic rutile (Rutile), Al-Jadeite (S-7); Cr-Synthetic chromium oxide Cr₂O₃ (S-14); Mg-Olivine (San Carlos-233); Fe-olivine (Fayalite-212); Ca-Diopside (Smithsonian); Mn-Spessartine (S-10); Na-Albite (Albite); K-Orthoclase (Orthoclase). Analytical results on standards are reported in Supplementary Information Table. More details of measuring conditions are available in Basak et al. 2023.

LA-ICPMS analyses

Trace element concentration including rare earth elements in whole rocks were obtained at the Material Science Department, Deutsches Bergbau-Museum Bochum, Germany. Sample digestion has been done with a µPREP-A microwave (MLS GmbH) after heating the powdered samples to dryness for 8 h at 105 °C. About 100 mg sample material have been digested in PTFE pressure vessels with 5 g HCl, 1,2 g HF and 5 g HNO₃, all concentrated, for 40 min at 250 °C. In the second step, 10 ml of 5% H₃BO₃ was added, and the solution again was heated up for 20 min. Finally, the digested samples were diluted with ultra-pure water up to 100 ml for a concentration of about 1000 mg/L. Chemical analyses have been performed with an SF-ICPMS (Thermo Fisher Scientific ELEMENT XR). For trace element analysis, sample solutions have been diluted 1:10 with 5% HNO₃. The analyses have been carried out with a FAST SC-system, ST 5532 PFA µ-FLOW nebulizer, Peltier-cooled PFA spray chamber and 1.8 mm sapphire injector in triple detector mode at the two different mass resolutions (low/middle) (m/Δm) depending on the elements of interest. Measurements have been controlled with standards BNV-1 (Basalt), DBC-1 (Ball Clay) and SBC-1 (Shale).

Trace element concentrations including rare earth elements in mineral phases such as garnet and plagioclase were



obtained using laser ablation inductively coupled plasma mass spectrometry (LA-ICP-MS) at the Institute for Mineralogy in the University of Münster, Germany. A pulsed 193 nm ArF excimer laser (Analyte G2, Photon Machines) with a spot diameter of 25 and 45 µm with a repetition rate of 10 Hz was used to ablate the minerals. A ThermoFisher Scientific Element 2 mass spectrometer was used for the analyses. A repetition rate of 10 Hz was used throughout the session. Elemental analysis was performed using an Element 2 mass spectrometer (ThermoFisher Scientific). The forward power was set to 1300 W, with reflected power kept below 1 W. Gas flow rates were maintained at 1.2 L/min for He (carrier gas for ablated material), 0.9 L/min for Arauxiliary gas, and 1.2 L/min for the sample gas. The cooling gas flow rate was adjusted to 16 L/min. Prior to analysis, the system was tuned by optimizing the torch position, lenses, and gas flows using an NIST 612 glass standard, measuring ¹³⁹La, ²³²Th, and ²³²Th¹⁶O to ensure stable signals, high sensitivity, and low oxide formation ($^{232}\text{Th}^{16}\text{O}/^{232}\text{Th} < 0.1\%$) during ablation. 43 elements were quantitatively analysed in total using the NIST 612 glass as an external standard. As an internal standard ²⁹Si (SiO₂ in garnet: 37 wt%, plagioclase: 60 wt%) was used, concentration of which was previously determined from the electron microprobe analyses in RUB. The data were processed using Glitter software (Griffin 2008). The standard reference glasses BHVO2-G and BIR1-G were analysed to monitor precision and accuracy for silicate phases throughout this study. The obtained results align with the published concentration ranges in the GeoReM database (version 23) (Jochum et al. 2005).

U-Pb and trace element analyses in zircon and rutile

Zircon mounts were prepared in the laboratories of Ruhr University Bochum, Germany. The preparation process began with crushing the samples using a jaw mill, followed by sieving with meshes of varying sizes. Magnetic minerals were then separated using an isodynamic separator. Zircon grains were isolated through panning, first in water and later in ethanol. Since minerals such as rutile and apatite were often present even after magnetic separation and panning, the samples underwent acid treatment in the laboratory to facilitate manual selection. The acid treatment involves placing the samples in hydrochloric acid (37%) and hydrofluoric acid (40%), then heating them on a hot plate at 300 °C. Individual zircon grains were then handpicked under a binocular microscope and embedded in epoxy discs. Rutile mounts were prepared following the same procedure but excluding the acid treatment step for U-Pb analyses.

Following the method described in Gerdes and Zeh (2006,2009) a ThermoScientific Element XR sector field ICP-MS coupled to a RESOlution-LR ArF Excimer laser

system at FIERCE, Goethe-University Frankfurt was used to analyse U, Th and Pb isotopes and element concentrations in the zircons. Ablation was carried out with an energy density below 2 J/cm² at a frequency of 6 Hz, using spot sizes of $20{\text -}30~\mu\text{m}$. The resulting penetration depth was approximately 15 μ m for a 20-second ablation period.

Common Pb correction was performed using ²⁰⁸Pb_c, after accounting for ²⁰⁸Pb produced by ²³²Th decay, and applying the Pb composition model of Stacey and Kramers (1975). In most cases, common Pb levels were low (e.g., <0.5% ²⁰⁶Pb_c of total ²⁰⁶Pb), and the correction remained within the uncertainty range of the uncorrected age. Downhole fractionation of ²⁰⁶Pb/²³⁸U was corrected individually for each analysis using a linear regression with a zero-time intercept.

The primary zircon reference material (RM) used was GJ-1 (²⁰⁶Pb/²³⁸U: 603.3 Ma; ID-TIMS age, W. Doerr, personal communication). Additional RMs, including BB-16 (Santos et al. 2017), 91,500 (Wiedenbeck et al. 1995), and Plešovice (Sláma et al. 2008), were used for validation. The weighted average ²⁰⁶Pb/²³⁸U ages obtained for these RMs- 561.7 ± 2.1 Ma, 1066.4 ± 4.0 Ma, and 338.9 ± 1.3 Ma (n=27, based on two analytical sessions)—were within 0.8% or better of reported values. Reported ²⁰⁶Pb/²³⁸U uncertainties (2σ) were propagated by quadratically adding excess scatter observed in GJ-1 (n=14 per session), within-run precision of individual measurements, and uncertainties from gas background and counting statistics. Concordia diagrams (2σ), concordia ages, and upper intercept ages (95% confidence level) were determined using Isoplot/Ex 2.49 (Ludwig 2001).

The same ICP-MS and laser system at FIERCE was employed for zircon trace element analysis. Isotope measurements for 25 elements were conducted in peak-jumping mode with a 30 µm spot size, fluence of 3.5 J/cm², and a 10 Hz repetition rate. Each analysis included a 25-second background acquisition followed by 35 s of data collection. Data reduction was performed using GLITTER 4.0, employing ²⁹Si (15.2 wt%) as the internal standard and NIST SRM-612 glass as the external calibration standard. To identify inclusions, elements such as P, Ca, Ti, and Sr were monitored, and data exhibiting unusually high signals were discarded from the time-resolved profiles. Eight spot analyses of the GJ-1 zircon reference showed a precision of 3-11% for REEs (>20 ppb), Y, Sr, Ti, Nb, Ta, Hf, U, and Th, aligning with the precision and accuracy obtained from seven analyses of the 91,500 zircon.

Garnet Lu-Hf analyses

Garnets separates were handpicked using a stereomicroscope after crushing the sample and sieving them into different fractions of magnetic and non-magnetic minerals using



an isodynamic separator in RUB. The separates were treated with 2.5 M HCl in an ultrasonic bath and rinsed twice with deionized water in the laboratories of University of Cologne, Germany before sample preparation for their isotopic analyses. Following the chemical protocol mentioned in Münker et al. 2001; samples were treated and then Lu-Hf were separated. Isotopic compositions were obtained using Thermo Fischer Neptune© or Thermo Fischer Neptune Plus© MC-ICP MS in Cologne. 179Hf/177Hf of 0.7325 was used for correction of mass bias. The measured ¹⁷⁶Hf/¹⁷⁷Hf ratios are given relative to the AMES standard that has a 176 Hf/ 177 Hf ratio of 0.282160 (Münker et al. 2001). For the dilution measurements of Lu isotopes, ¹⁷³Yb/¹⁷¹Yb ratios of 1.29197 were used to perform mass bias corrections. The external reproducibilities of Hf isotopes amount to ± 40 ppm and 176 Lu/ 177 Hf ratios amount to $\leq 0.2\%$ (2RSD). These garnet separates were measured together with other samples, data of which including information on external reference are published in Hasenstab et al. 2021. More details on sample preparation and measurement conditions are available in Basak et al. 2023. Age regressions were calculated using ISOPLOT (Ludwig 2001) and using a decay constant for ¹⁷⁶Lu of 1.867 × 10−11 year⁻¹ (Scherer et al. 2001; Söderlund et al. 2004).

Ti in zircon thermometry

Rocks which have cogenetic zircon, rutile and quartz are suitable for using the thermometer as then the a_{SiO2} and a_{TiO2} may be set equal to 1. The expression for the thermometer (Ferry and Watson 2007) is as follows:

$$\log Ti = (5.177 \pm 0.072) - ((4800 \pm 86)/T(K))$$

Phase equilibrium calculations (see below) indicate that rutile was present at all stages during the evolution of the rocks at high temperatures. We have calculated temperatures with 2 σ error bars during zircon crystallization using equation A for the metapelite and leucosome in context to different textures and age groups.

Thermodynamic modelling

The phase equilibria diagram for the metapelite was calculated with the software Perple X '98 in the sys-Na₂O-CaO-K₂O-FeO-MgO-Al₂O₃-SiO₂-H₂O-TiO₂ (NCKFMASHTi) using the Perple X software version 7.1.1 (Connolly 2005 with further updates) along with the internally consistent thermodynamic dataset of Holland and Powell (2011). The following mineral solid solutions models were used in the calculations: spinel (White et al. 2000), garnet, orthopyroxene, staurolite, cordierite, chlorite, chloritoid, biotite and white mica, ilmenite-haematite, silicate-melt (White et al. 2014), feldspar (Fuhrman &

Lindsley 1988), and epidote (Holland and Powell 2011). Mineral abbreviations after Kretz (1983). As the pelitic rock has leucosome material mixed with it on a grain scale, it is difficult to obtain a reliable chemical analyses of the rock. Therefore, we have used effective bulk rock composition which is calculated using the measured mineral compositions with calculated modal abundances to obtain the bulk compositions of the rocks. Modal proportions of the constituent minerals were quantified using point counting on high-resolution thin section scans in JMicroVision (Roduit 2025), allowing for accurate estimation of volume fractions (Supplementary Material Fig. 2). Reasonable variations of modal abundances do not alter the results of phase equilibrium calculations reported below significantly. All calculations with varying modal abundances for effective bulk and with measured bulk in different systems with varying water content are provided in Supplementary Material Fig. 3.

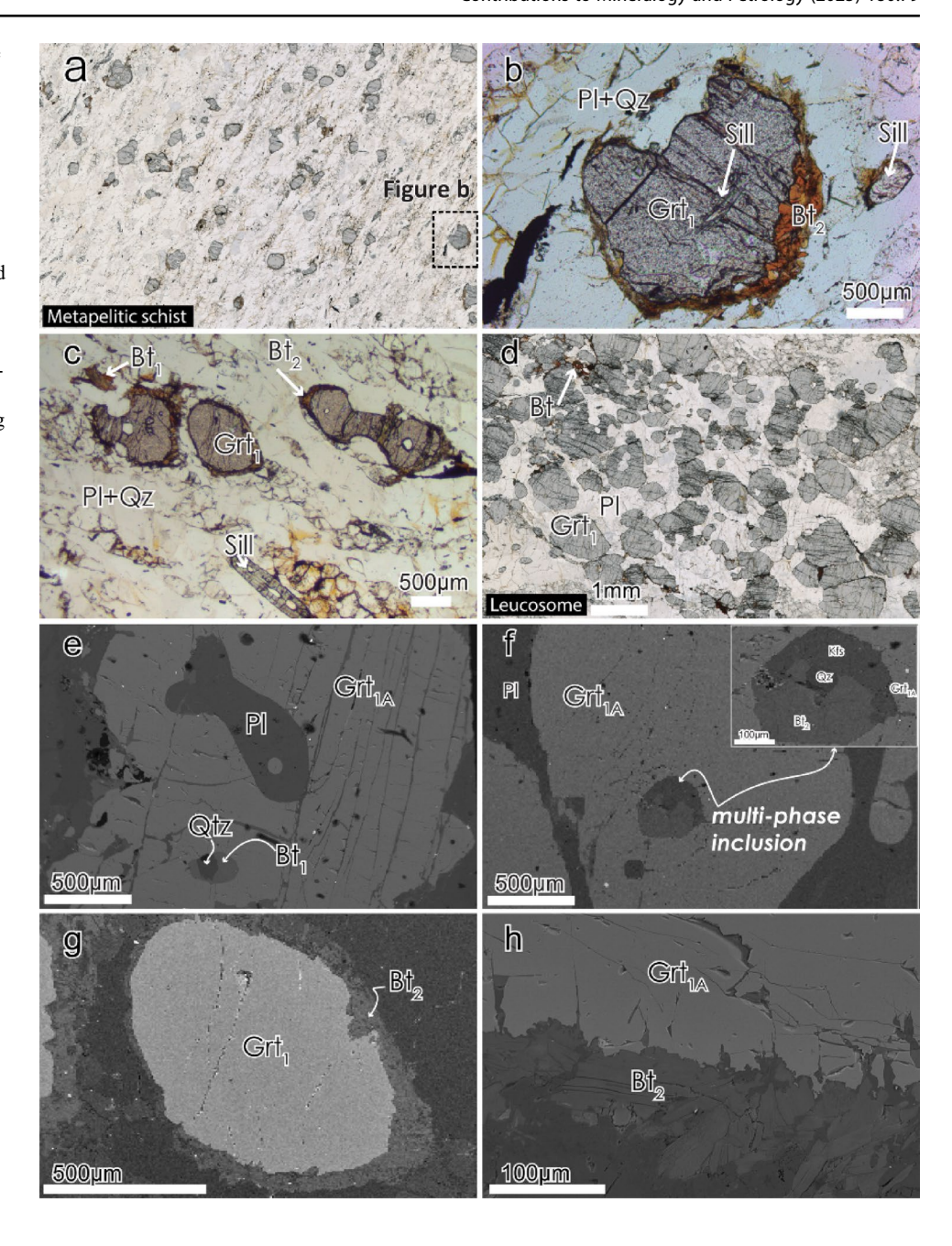
Results

Petrography

The main pelitic lithology from the exposure sample consists of garnet bearing sillimanite-biotite-plagioclasequartz-rutile metapelite. The main foliation is defined by the oriented and elongated sillimanite grains (Fig. 2a). Many garnet grains, Grt₁, are elongated with their long axes oriented parallel to the gneissic foliation and they are mostly free of inclusions. A few occurrences of sillimanite (Fig. 2b), and rarely biotite, as inclusions in garnet (Grt₁) are found along with some ilmenite and magnetite. Biotite is mostly absent from the main foliation domain except for the occurrence of a few grains, Bt₁ (Fig. 2c). The above-mentioned metapelite is closely associated with a quartzo-feldspathic counterpart that we term leucosome. It consists of garnets in a matrix of plagioclase, quartz, and minor amount of potassium feldspar. Figure 2d is a thin section scan of the representative sample. These garnets, hereby termed as Grt_{1A} are mostly rounded and devoid of inclusions, but significantly, they contain multi-phase inclusions of biotite, potassium feldspar and quartz together in some grains (Fig. 2e, f). In the leucosome, texturally there are two populations of garnet grains - one smaller, rounded and less than 100-200 micrometer in diameter; the other population of grains are much bigger, ranging to millimeters in diameter. Accessory minerals in these rocks are rutile and zircons. There are numerous fractures parallel to both long and short axes of the garnet grains. Secondary biotite has filled such fractures in certain places or have rimmed the garnet grains. The second type of biotite, Bt2, is mainly present as intergrowths of



Fig. 2 a Thin section scan in plane polarised light of the metapelite (CM 27C-17); b shows porphyroblastic Grt₁ from (a) showing the relict sillimanite inclusions as well as retrograde second generation biotites rimming Grt₁ (Bt₂); c shows the stable mineral assemblage of the metapelite; d thin section scan in plane polarised light of the leucosome (CM 27B-17) showing the abundance of garnets (Grt_{1A}); \mathbf{e} and \mathbf{f} shows Grt_{1A} present in leucosomes showing polyphase melt inclusions; with an enlarged view highlighting the details of the melt inclusion; g and h show the second generation biotite (Bt₂) rimming Grt_{1A} in the metapelite and leucosome respectively



thin flakes of biotite and quartz forming rims along almost all of the elliptical or circular garnet grains (Fig. 2g, h).

Major and trace element compositions of minerals

Garnet

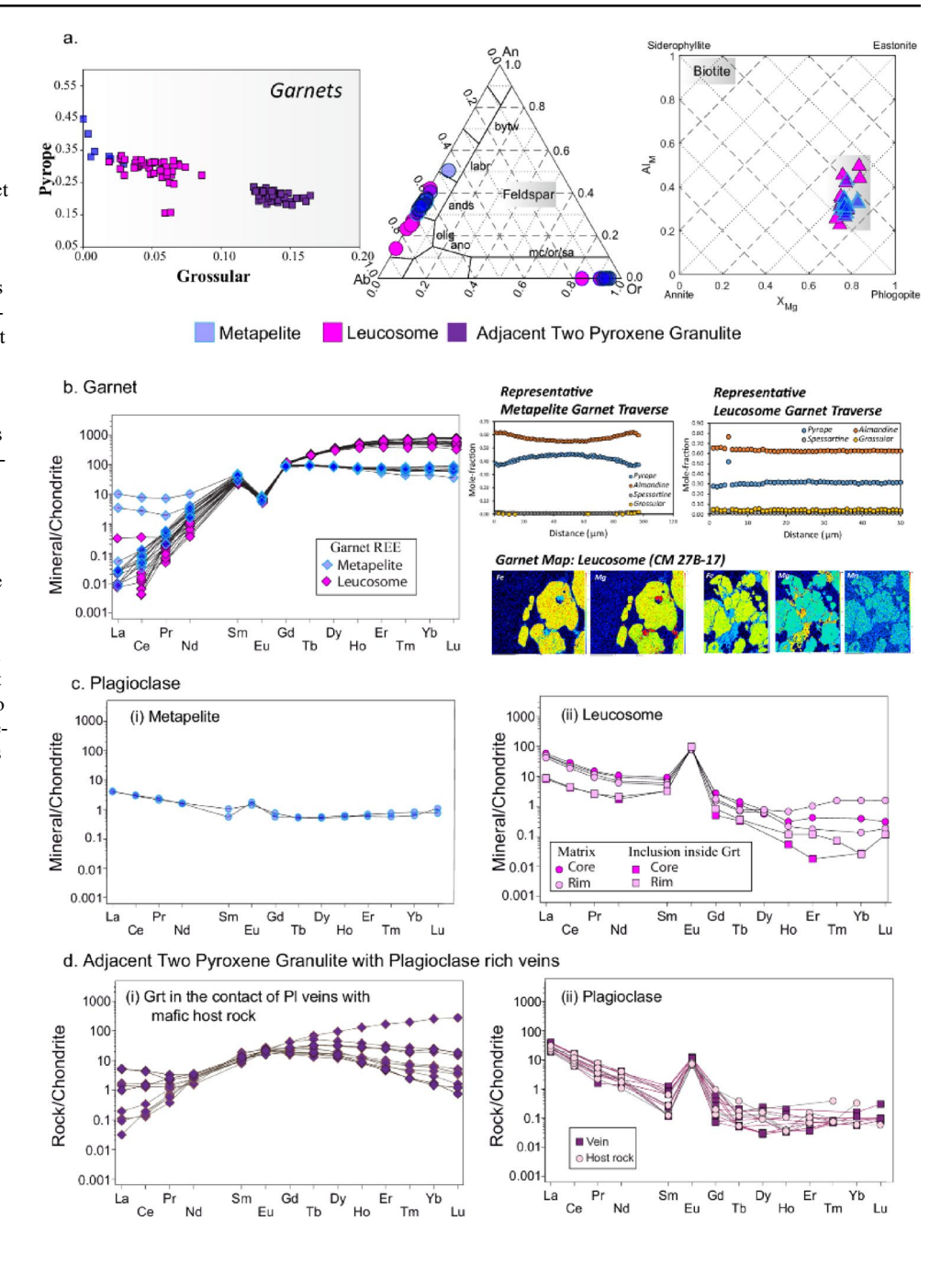
The average composition of garnet (Grt_1) in the metapelite (sample CM 27C-17) is $Prp_{0.44}Alm_{0.55}Sps_{0.009}Grs_{0.001}$ in the core and $Prp_{0.33}Alm_{0.64}Sps_{0.01}Grs_{0.02}$ in the rim (Fig. 3a, Supplementary Information Table 2a) with X_{Mg} values of 0.44–0.46 in the core to 0.29–0.36 in the rim. The rare earth element (REE) compositions have been measured from the

core, intermediate and rim regions of individual grains (Supplementary Information Table 3a). The chondrite normalized REE plot for Grt₁ normalized using concentrations in chondrite from Sun and McDonough (1989), shows LREE depletion with respect to HREE and high concentration yet flat normalized pattern in HREE with a distinct negative Eu anomaly (Fig. 3b). These garnet compositional features are common for core-rim variation, although in some grains there is an enrichment in LREE in the rims in comparison to the HREE (Fig. 3b).

For the leucosome (sample CM 27B-17), the garnet (Grt_{1A}) composition varies from Prp₃₂Alm₆₂Sps₂Grs₄ in the core to Prp₂₄Alm₆₇Sps₂Grs₇ in the rim (Fig. 3a and



Fig. 3 a Binary plot showing pyrope-grossular compositional variation within different garnets from both the metapelite (CM 27C-17) and the leucosome (CM 27B-17), also compared with the garnets (Grt₂) formed at the contact of plagioclase rich melt veins and the adjacent host two pyroxene granulite (Basak et al. 2023). In addition, classification of feldspars and biotite are shown: b The chondrite normalized rare earth element (REE) patterns of garnets from metapelite (CM 27C-17) and leucosome (CM 27B-17) are shown along with representative traverses of garnets from metapelite and leucosomes and representative major element maps of garnets from leucosomes; c Chondrite normalized REE patterns of plagioclase from i metapelite and ii leucosome are shown; **d** For comparison, chondrite normalized plots of garnets (Grt₂) and ii plagioclase (both vein and matrix) from the adjacent mafic rock (CM 27D-17) have also been plotted, data of which are presented in Basak et al. 2023. Values for chondrite normalisation are from Sun and McDonough (1989)



Supplementary Information Table 2b). There is a small but distinct difference in the garnet core composition of the larger grains, $Py_{32-35}Alm_{62-64}Sps_2Gr_{0.3-0.4}$, vs. the smaller grains, $Py_{30-32}Alm_{62-65}Sps_2Grs_{0.4-0.6}$ with X_{Mg} values of 0.31–0.34 in the core to 0.29–0.34 in the rim. The chondrite normalized REE patterns of leucosome garnet grains show an enrichment in HREE with respect to LREE with a prominent negative Eu-anomaly (Fig. 3b and Supplementary Information Table 3b). The results are the same from all textural domains, with isolated garnet rim compositions showing, once again, an enrichment in LREE in comparison to HREE. (Fig. 3b). Representative profile of garnet

from metapelite and leucosome along with representative major element map of garnets from the leucosome is also provided in Fig. 3b. In mafic granulites, garnets (Grt₂) (second generation garnets, as defined in Basak et al. 2023) are mostly grossular rich and pyrope poor (core Prp₁₉Alm-62Sps₂Grs₁₆ and rim Prp₂₂Alm₆₃Sps₂Grs₁₂) (Fig. 3a, data presented in Basak et al. 2023) with numerous inclusions of mostly quartz but also amphiboles, as compared to the ones in the metapelite and the leucosome. The REE content of Grt₂, both core and rim (data presented in Basak et al. 2023) shows no compositional variation. The chondrite normalized REE pattern is quite distinct with an enrichment of



MREE as compared to LREE and HREE. Also, HREE are slightly more enriched than LREE (Fig. 3d, i). In all cases there is no Eu anomaly.

Plagioclase

The plagioclase grains surrounding garnet (Grt_1) in the metapelite are calcium rich andesine, $An_{37}Ab_{62}Or_2$. (Fig. 3a, Supplementary Information Table 4). The plagioclase in the metapelite shows a moderate enrichment in LREE compared to HREE, with a slight positive Eu anomaly in the rim (Fig. 3c (i)).

In the leucosome, plagioclase cores and rims are andesines, An_{31–35}Ab_{64–68}Or_{1–2}. A core-rim variation is absent there (Supplementary Information Table 4). Plagioclase from two textural settings (matrix and inclusions within garnet) shows a slightly enriched LREE and depleted HREE pattern with a positive Eu anomaly, but the enrichment is more pronounced in the matrix plagioclase (Fig. 3c(ii), Supplementary Information Table 5). The HREE in both kinds of plagioclase show a generally flat pattern with some scatter.

The composition of plagioclase of the adjacent mafic rock in the matrix of the host rock is An₃₁₋₃₃Ab₆₆₋₆₈Or₁ whereas the composition of plagioclase in the leucocratic vein in the mafic rock is An₂₈₋₃₀Ab₆₈₋₇₀Or₃₋₄ with no significant core-rim variation in the grains from both the textural settings. The plagioclase REE pattern is quite similar in the felsic (this study) to the ones obtained from plagioclase grains in both the textural settings in the mafic rocks (Basak et al. 2023), with LREE enriched compared to the HREE and a positive Eu anomaly (Fig. 3d(ii) and data presented in Basak et al. 2023).

Biotite

Biotite is present in the metapelite in three textural settings (composition in Supplementary Information Table 6a): (i) as inclusion inside the garnet porphyroblast ($X_{\rm Mg}$ = mol Mg/(mol Mg+mol Fe)=0.82-83; Ti (a.p.f.u.)=0.12-0.13), (ii) as few grains in the matrix, Bt₁, ($X_{\rm Mg}$ = 0.76-0.77; Ti (a.p.f.u.)=0.17-0.20) and (iii) as rims surrounding the garnets, Bt₂, ($X_{\rm Mg}$ = 0.76-0.77; Ti(a.p.f.u.) (core)=0.16-0.17). The leucosome rock also has biotite in two textural settings (composition in Supplementary Information Table 6b): (i) as a mineral inclusion inside the garnet grain (core: $X_{\rm Mg}$ = 0.74-0.78; Ti (a.p.f.u.)=0.08-0.18; and (ii) as rim surrounding the big garnet porphyroblast (core: $X_{\rm Mg}$ = 0.75; Ti (a.p.f.u.)=0.13).

Metamorphic history

Mineral reactions

The **M1 event** is defined by vestiges of fibrolitic sillimanite inside the garnets (Grt₁) and earlier biotite grains (Bt₁) in the metapelite indicate that they may have been involved in the formation of the garnet crystals that are currently seen in the rock (Fig. 2b, c). The growth of garnet porphyroblasts may have occurred because of an increase in temperature resulting in biotite dehydration reaction such as:

$$Bt_1 + Sill + Pl \rightarrow Grt_1 + Qtz$$
 (1)

This reaction marks the metamorphic event (M1). The above is written as a model reaction; in order to balance the reaction a fluid/melt phase with K would be necessary (Breton and Thompson 1988; Patiño Douce and Beard 1995).

The **M2 event** is defined by the presence of high-Ti biotite, K-feldspar and quartz inside the garnet grains observed in the leucosome (Fig. 2e, f) which indicates that possibly with subsequent heating and increase in pressure, the metapelite crossed its solidus temperature causing melting following the reaction:

$$Bt_1 + Sill + Pl + Qtz \rightarrow Grt_{1A} + K - feldspar + Melt$$
 (2)

This reaction marks the metamorphic event (M2). While we have distinguished the two reactions based on their location of occurrence (metapelite vs. leucosome), they may well represent a single metamorphic event of biotite dehydration with different imprints in different local bulk compositions.

The subsequent metamorphic **M3A event** that is recorded is the rimming of Grt_1 and Grt_{1A} by late stage growth of biotite (Bt₂), quartz intergrowth in the leucosome and metapelite (Fig. 2g, h). These biotite selvedges have often been interpreted as a result of melt rock interaction during cooling (Spear 2004) leading to the reversal of the following reaction (2) which marks the metamorphic event (3 A):

$$Grt_{1A} + Melt + Kfs \rightarrow Bt_2 + Pl + Qtz$$
 (3)

The mafic rock associated with the pelitic rocks records the evidence of formation of a texturally and compositionally different generation of garnet at the contact of the host rock with the leucocratic vein. We tentatively assign this stage of fluid/melt influx and reaction as the M3B event, based on observations reported in Basak et al. 2023 on these kinds of rocks from the same region.

The final **M4 event** in the P-T history is likely to be preserved by the retrograde exchange compositions of garnet (Grt₁ and Grt_{1A}) and biotite (Bt₂) in contact with each other.



Thermobarometry

One of the key challenges for determining pressure and temperature conditions of metamorphism in rocks that have undergone partial melting, melt segregation and multistage metamorphic evolution, and contain zoned minerals, is the choice of mineral compositions to carry out the calculations keeping kinetic constraints in mind (Dasgupta et al. 2009; Sorcar et al. 2014; Zhao and Chakraborty 2024). In the metapelite, it is difficult to quantify the P-T conditions of the M1 metamorphic event due to the obliteration of most of the matrix biotite, where "matrix" refers to the biotite present away from the garnet grains and not in close contact. This process of an "infinite" reservoir of biotite (i.e. high modal abundance of biotite relative to garnet) from the foliation domain is necessary for thermobarometric calculations because this ensures that compositional change during Fe-Mg exchange is accommodated by changes in composition of garnet only, while the biotite composition stays fixed (e.g. Ferry and Spear 1978). In rocks with low modal abundance of biotite one can obtain spurious temperatures in such circumstances (e.g. Spear and Markussen 1997). For the M2 event, we have chosen the Ti in zircon thermometry to derive the recorded maximum temperature attained by the rock which is discussed later in the text after classification of different kinds of zircons present in the rock. The M3A event may be quantified using the breakdown of garnet to form new biotite grains using appropriate phase diagrams (see below). One of the advantages for thermobarometric calculations for these rocks is the presence of three different rock types at the same exposure. The mafic rock (belonging to mafic granulite group A1 with low magnesian bulk rock composition of Basak et al. 2023) which was found intercalated with the supracrustals gives a calculated P-T value of 620–720 °C, 7–8 kbar, using the Garnet-Clinopyroxene thermometer (Ganguly et al. 1996) and the Garnet-Clinopyroxene-Plagioclase-Silica barometer (Eckert et al. 1991) for the M3B event.

The Fe-Mg thermometer following the formulation of Ganguly et al. (1996) applied to the rim compositions of garnets and the immediately adjacent compositions of biotite in both the leucosomes and the metapelite constrain the temperatures in the M4 event. The calculated temperature ranges from 499 to 562 °C with an average of 533±42 °C (Supplementary Information Table 7) in the metapelite and from 445 to 525 °C with an average of 494±52 °C in the leucosome at a reference pressure of 6 kbar. The temperature range shifts very little if calculations are carried out at other pressures (e.g. 506-569 °C for the pelites and 452-532 °C for the leucosome if a reference pressure of 8 kbar is considered). We have also calculated the temperatures using the original experimental calibration of Ferry and Spear (1978) (i.e. without the more recent activity models for garnet and pyroxene) for comparison, and the results obtained are similar within uncertainty. The pressures obtained from the GASP barometer using the garnet rim compositions and adjacent plagioclase compositions (An₃₇) lie in the range of 5-6 kbar, but the significance of these values is considered below.

Pseudosection modelling and overall constraints on pressure and temperature at different events

The calculated phase diagram (Fig. 4a) was modelled using effective bulk composition using calculated modal abundances of each phase and respective mineral chemistry (Supplementary Information Table 8). The figure shows the boundary of kyanite-sillimanite phase transition marked in dotted black lines along with the cordierite-out and biotiteout line highlighted as a dotted line as well and the solidus marked as a dotted red curve. Various modal abundances and compositional isopleths of phases were also determined (Fig. 4b and c). The isopleths of $X_{\mbox{\scriptsize Mg}}$ of garnets as well as its modal abundance are also plotted on Fig. 4b and c to indicate clearly where growth and breakdown of the phase occurs during melting and recrystallization. The absence of kyanite and cordierite in the sample marks the upper and lower pressure limits of the evolutionary path of the rock. With increase of temperature, the modal abundance of garnet increases from 10 to 24% and $X_{\mbox{\scriptsize Mg}}$ values from 0.35 to 0.46. The near elimination of biotite by the melting (reaction 2) beyond the solidus, the X_{Mg} of garnets, absence of kyanite and Ti-in zircon thermometry (see below) together help us to constrain the location of the M2 event in P-T space. The M3 event is simultaneously constrained by Ti in zircon thermometry of zircon rims (reaction of melt with garnet to form biotite by reaction 3, M3A event) as well as the thermobarometry and phase equilibria constraints on the associated mafic rocks (M3B event) at ~620-720 °C and \sim 7–10 kbar (Basak et al. 2023). Finally, the M4 event is marked by the retrograde readjustment of compositional zoning of garnet at its rim in contact with biotite to yield the final freezing temperature of Fe-Mg exchange between garnet and biotite at ~500 °C. The pressure at this event remains somewhat equivocal. The use of plagioclase compositions near the same rims of garnet in GASP barometry yield pressures as high as 5-6 kbar. However, it is unclear if the plagioclase compositions reflect the compositions at the time of garnet breakdown (M3 event) or at the time of freezing of the Fe-Mg exchange (M4 event). Pressures as high as 6–7 kbar in the M4 event should have stabilized kyanite in the reaction rims, for which there is no evidence. Therefore, the history between M3 and M4 events may have been one of nearly isobaric cooling (where phases such as kyanite



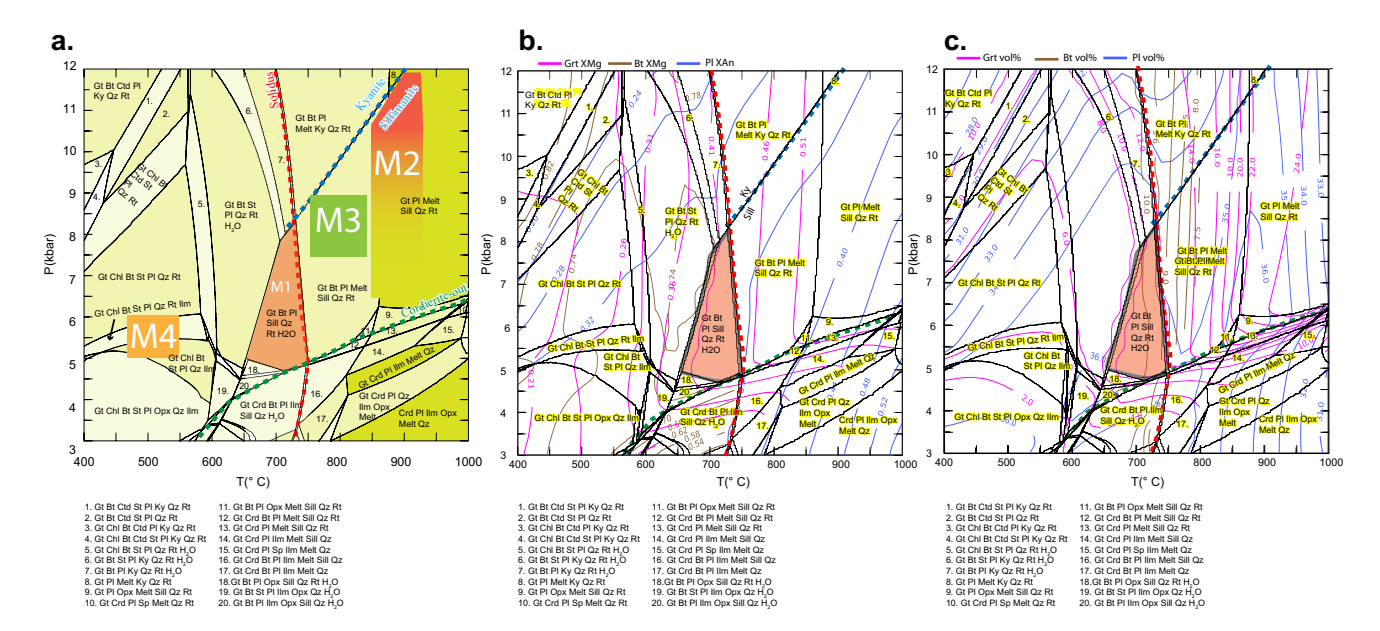


Fig. 4 a Phase equilibria diagram calculated using effective bulk compostion using mineral composition and modal abundance as shown in Supplementary Information Table 8; **b** Compositional isopleths of major mineral phases were plotted based on the pseudosections calculation. X_{Mg} is calculated as $Mg/(Mg+Fe^{2+})$ and X_{Ca} is calculated as Ca/(Ca+Na). The P-T conditions of different events are also

marked. See text for details; **c** Contours of the modal abundance (vol %) of major mineral phases calculated using the werami software of Perple_X. The stable mineral assemblage of plagioclase-garnet-sil-limanite-biotite-quartz-rutile is marked. The different metamorphic events derived from the mineral reaction history are also indicated in **(a)**. See text for details

did not form due to metastability or effects of local bulk compositions), or one of decompression and cooling (in which case the barometric results based on the plagioclase compositions at the rim are incorrect for reasons discussed above). We consider both possibilities in the subsequent interpretations.

U-Pb studies of accessory minerals

Zircon texture, U-Pb geochronology and trace elements

The zircons from the metapelite (sample CM 27C-17) are White to translucent. They are mostly ellipsoidal to circular with grain sizes from 50 to 250 µm and length to width ratio between 1:1 to 2:1. As seen under transmitted light, some of the grains have inclusions, or a very dark outer rim. Cathodoluminescence imaging reveals a distinct corerim structure (Fig. 5a). The cores preserve oscillatory zoning whereas the rims are darker and show no zoning with mostly uniform thickness.

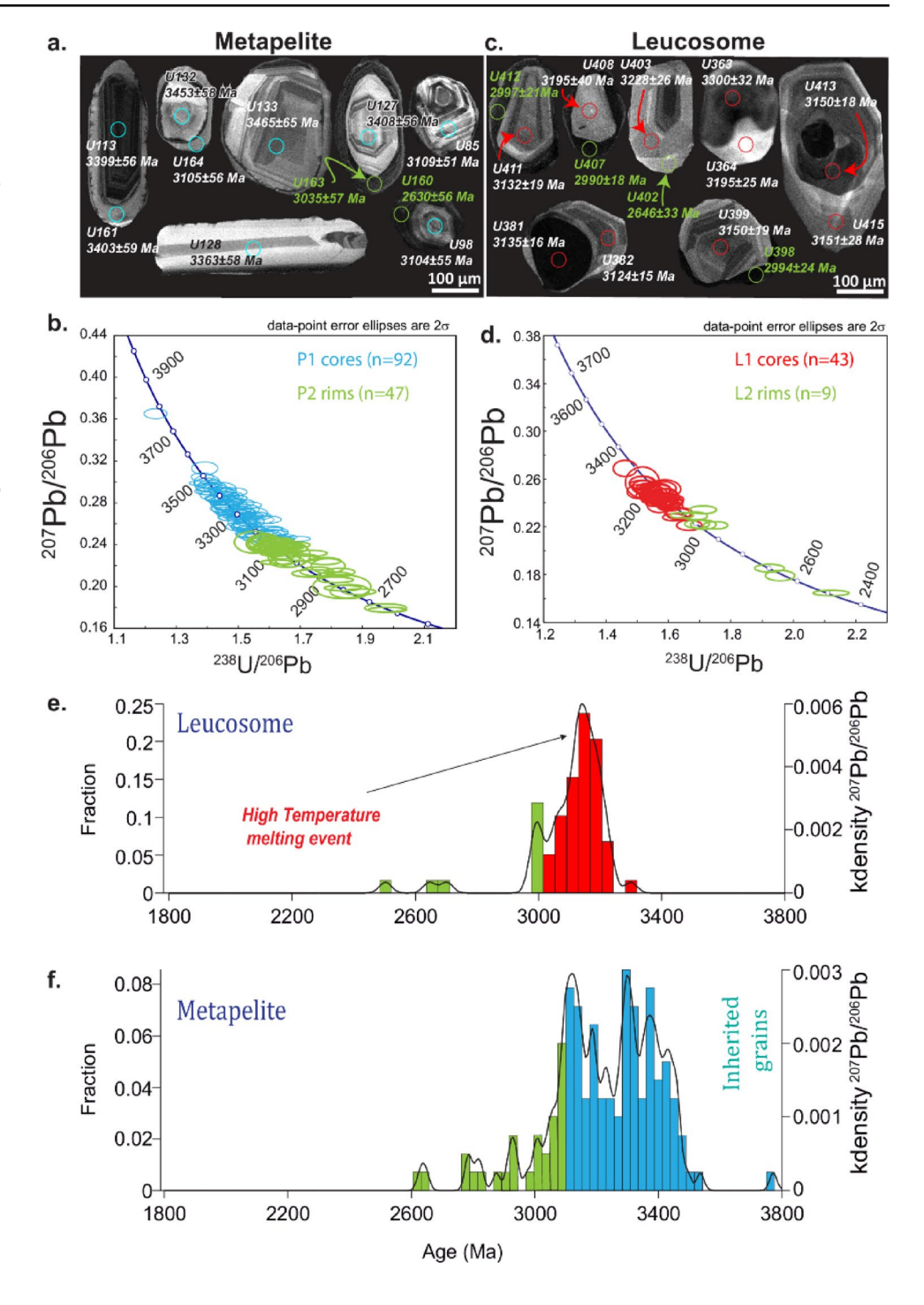
In total, 151 U-Pb analyses from the metapelite are divided into three categories (see Supplementary Information Table 9) based on age, texture, concordance, and rare earth element abundances. The detailed description of each group is as follows: Group P1 consists of analyses conducted mostly on zircon cores (marked with open blue circles in Fig. 5b). U-Th-Pb measurements on 84 zircons were made. They yield low to moderate U (6.2–285 ppm)

and Th (2.5-449 ppm) with Th/U=0.19–2.10. The concordant $^{207}\text{Pb}/^{206}\text{Pb}$ dates range from 3149 to 3536 Ma. A single zircon in this group gives an older date of 3772 ± 72 Ma. Its U and Th content is at 27 and 13 ppm, respectively with a Th/U ratio of 0.5. Group P2 (marked in green open circles, in Fig. 5b) represents the zircon dates which were obtained mostly by analyzing the darker rims. They yielded low to moderate U (36-333 ppm) and Th content (7.1-270 ppm) with Th/U ratios of 0.033-2.12. The range of dates (n=47) fall within 2629-3141 Ma with 40 analyses in the range of 2914-3141 Ma, whereas the remaining seven analyses have a range from 2629 to 2874 Ma. Group P3 represents all the discordant data in the Terra-Wasserburg plot with concordance < 95%, which are interpreted as affected by Pb loss.

In the metapelite, we have measured REE concentrations of 45 zircon domains from the groups as described above (Supplementary Information Table 10a). Group P1 zircon shows positive Ce anomaly (Ce/Ce*= Ce_N/(La_N*Pr_N)0.5=21-141) and enriched HREE (high Lu_N/Gd_N ratio=14.50-52.12) with a negative Eu (Eu/Eu*=0.32-0.83) anomaly (Fig. 6a). These indicate zircon crystallization from the magma (or anatectic melt). Based on REE content and chondrite normalized REE patterns, Group P2 zircons can be further divided into 2 A and 2B. Textural rims of most zircons from Group P2A (Fig. 6a) give a different chondrite normalized REE pattern with a positive Ce and a stronger negative Eu anomaly (Ce/Ce*=1.44-38.59, Eu/Eu*=0.07-0.23) and depleted HREE pattern (low Lu_N/



Fig. 5 a Cathodoluminiscence images of zircon crystal from metapelite (CM 27C-17). The circles show LA-ICPMS analysis spots and corresponding U-Pb dates. For interpretation of the colours of the open circles used to indicate the analyses spots, refer to the text; b Terra Wasserburg diagram for U-Pb zircon analyses of the metapelite; c cathodoluminiscence images of zircon crystal from leucosome (CM 27B-17). For interpretation of the different groups refer to the text; d Terra Wasserburg diagram for U-Pb zircon analyses of the leucosome; e and f Frequency and density distribution of U-Pb zircon ages from the leucosome (CM 27B-17) and the metapelite (CM 27C-17) respectively



Gd_N= 0.66–34.85) with respect to that of Group P1. This pattern is suggestive of crystallization at metamorphic conditions in a garnet bearing assemblage. All the zircons have crystallized in the presence of plagioclase which incorporates Eu in its structure, resulting in strong negative Eu anomaly in the zircon. Variable magnitude of the anomaly could have resulted from a change in the modal abundance of plagioclase during evolution, or variations in the abundance of plagioclase in the local melt pool from which the

zircons grew. The range of dates in these zircons lie between 2783 and 3118 Ma which corresponds to Group P2A dates. We also found another group of zircons (Group P2B), representative U-Pb dates ranges of which lies between 2630 and 3034 Ma which also corresponds to the lower limit of Group P2 age range when total dates are considered. These are analyses of zircon rims showing a different REE with an enrichment in LREE ($La_N/Sm_N=0.58-2.14$) with respect to Group P1 and P2A and Eu/Eu* = 0.32–0.89. The relatively



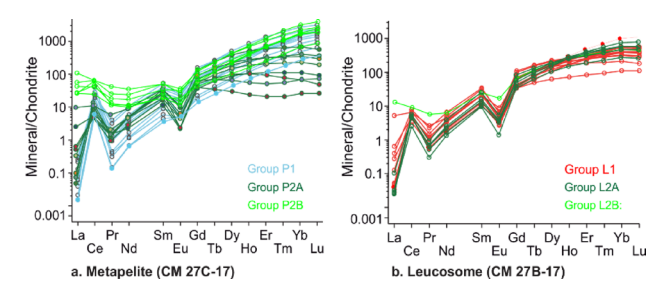


Fig. 6 Chondrite normalized REE plots of zircons from different textures for a Metapelite and **b** leucosome. See text for details. Data on REE patterns and trace element contents from the zircons in this study are presented below using the same colour code that was developed in the previous section to classify different populations according to texture and U-Pb age

higher LREE of Group P2B compared to the other groups suggest hydrothermal (Hoskin 2005) or some other mechanism of growth (Fig. 6a).

Zircons from the leucosome sample CM 27B-17 are light yellow to colourless. They are prismatic to ellipsoidal. The lengths range from 100 to 200 μ m, with length to width ratio ranging from 1:1 to 2:1. Cathodoluminescence imaging reveals that most of the grains have a dark rounded core (Fig. 5c) surrounded by a rim with oscillatory zoning. A few grain additionally have a darker outermost rim which is mostly<30 μ m in thickness.

In total 53 U-Pb measurements are divided into two categories (Supplementary Information Table 10), based on age, texture, concordance and different rare earth element patterns. Group L1 (marked in open red circles in Fig. 5d) corresponds to zircon cores and yields low to moderate U (37-218 ppm) and low Th (22-121 ppm) with Th/U=0.25–0.92. The concordant 207 Pb/ 206 Pb dates mostly range from 2989 to 3228 Ma. Only one zircon grain in this group gives an older concordant date of 3300±32 Ma. Its U and Th content is low at 39 and 25 ppm, respectively with a Th/U ratio of 0.63. Group L2 (marked in green open circles in Fig. 5d) represents the zircon dates which were obtained mostly by analyzing the dark outermost rims. The ²⁰⁷Pb/²⁰⁶Pb dates range within the overall date range of L1 except three concordant date of 2503 ± 19 Ma, 2646 ± 33 Ma and 2702±23 Ma. Group L3 represents the discordant data in the Terra Wasserburg plot with concordance < 95% and are interpreted as affected by Pb loss.

In the leucosome, REE measurements were done on twenty zircon domains from the groups mentioned above. The REE pattern of zircon domains from Group L1 is similar to magmatic zircon with moderately high HREE pattern (Lu_N/Gd_N = 2.66-28.10 and La_N/Sm_N = 0.01-0.2), negative Eu anomaly (Eu/Eu* = 0.10-0.24) and positive Ce anomaly (Ce/Ce* = 5.35-40.27). The pattern suggests growth of zircon in the presence of garnet and plagioclase. Representative REE analyses of the zircon rims (Group L2A) shows

similar features with respect to the garnet cores in terms of REE abundance except one zircon rim which gives a concordant date of 2503 ± 19 Ma (Group L2B) and shows different chondrite normalized REE pattern with higher LREE (La_N/Sm_N = 0.53) and lower negative Eu (Eu/Eu* = 0.42) anomaly with respect to cores (Fig. 6b).

Ti in zircon thermometry

In the metapelite, the pre-existing zircons from Group P1 have Ti concentration of 5.26-21 ppm and yield temperatures with range of 804–972 °C with an average of 850±30 °C (Supplementary Information Table 11). The zircon rims belonging to group P2 can be distinguished based on two distinct REE patterns. Group P2A have Ti content of 5.32–10.80 ppm and yield a temperature range of 805–885 °C with an average of 830±11 °C and corresponds to M3A-1 event (Supplementary Information Table 11). Ti content of zircon rims of Group P2B range from 4.35 to 7.09 ppm and yield a temperature range of 786–836 °C with an average of 815±24 °C and corresponds to both M3A-2 (~2813–3035 Ma) and M3B events (2630±56 Ma). (Supplementary Information Table 11).

The zircons from the leucosome CM 27B-17 which fall in Group L1 and corresponds to M2 event have a Ti range of 11.02-15.7 ppm which yield a temperature range of 850-933 °C an average of 900 ± 14 °C (Supplementary Information Table 11). Group L2A zircons with mostly younger dates show a Ti content of 6.55-12.6 ppm which yield a temperature range of 872-900 °C with an average value of 885 ± 20 °C and corresponds to M3A-2 event (~2990-2997 Ma which falls within the overall date range of L2). One L2B zircon with distinct REE pattern have a Ti content of 7.78 ppm and yield a temperature of 850 ± 20 °C (Supplementary Information Table 11) and corresponds to M3B event (2503 ± 19 Ma).

Lu-Hf garnet geochronology

A garnet population from the leucosome and one from the mafic rock was analysed for Lu-Hf geochronology (Supplementary Information Table 12; Fig. 8a). The date of the garnets in the adjacent mafic granulite (CM 27D-17) which corresponds to the second generation of garnet in the mafic granulites is 2450 ± 66 Ma (MSWD-45, Basak et al. 2023). Three garnet fractions were analysed and they represent garnet separated unbiasedly irrespective of their size. To better understand the extent of the effect from mixed garnet populations, we calculated isochron dates in two ways: (1) all the garnet fractions and the respective whole rock were included; and (2) two-point isochrons were calculated using the whole rock with each individual garnet fraction.



79

The three garnet fractions from leucosome CM 27B-17 yield an errorchron of 2863±140 Ma with a very large MSWD of 75. The calculated dates for the three two-point isochrons are 2811 ± 11 Ma, 2895 ± 11 Ma and 2925 ± 15 Ma respectively.

U-Pb ages of rutile

We have analysed U and Pb isotopes in the rutile grains obtained from the metapelites and the associated garnet bearing leucosome (Supplementary Information Table 13; Fig. 7b). In each sample the analyses form a single cluster within their analytical uncertainties. The rutile from the metapelite yield an average date of 612 ± 10 Ma (MSWD=1.29). The U-Pb date of the rutile analyses from the leucosome is 628 ± 10 Ma (MSWD=2.26), which is within uncertainty of the metapelite date.

Stability of zircon in melt

Given the physical association of the leucosome and the pelite in the field as well as the chemical affinity between the two (i.e. the leucosome as products of melting of the pelitic rock), the question that arises to: Why do the zircon populations in the two rocks differ in their age and trace element signatures. To evaluate this aspect, we have carried out calculations to evaluate how long zircons might survive in a melt at the relevant P-T conditions of metamorphism/ partial melting. For this modelling we have used the code

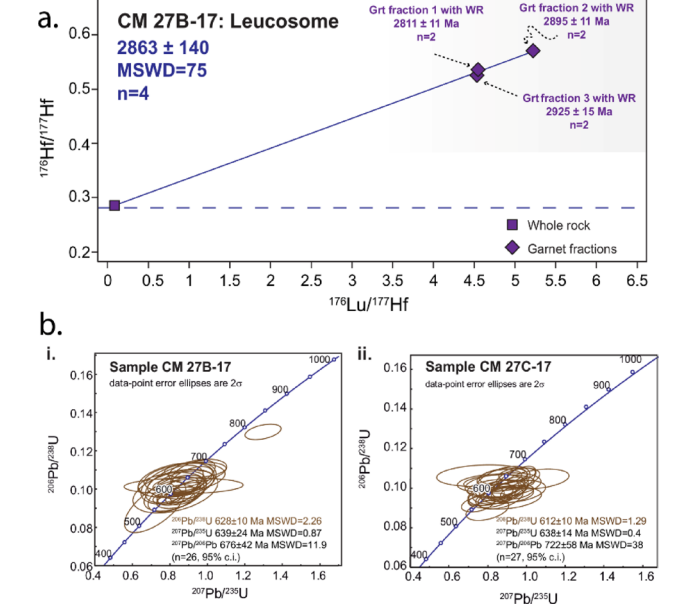


Fig. 7 a^{176} Lu- 176 Hf plots for three garnet separates from the leucosome and its whole rock. The Program 'ISOPLOT' (Ludwig 2001) was used to calculate isochron regressions using the errors reported in Supplementary Information Table 12; b U-Pb dates of rutile grains from the i Leucosome (CM 27B-17) and ii Metapelite (CM 27C-17)

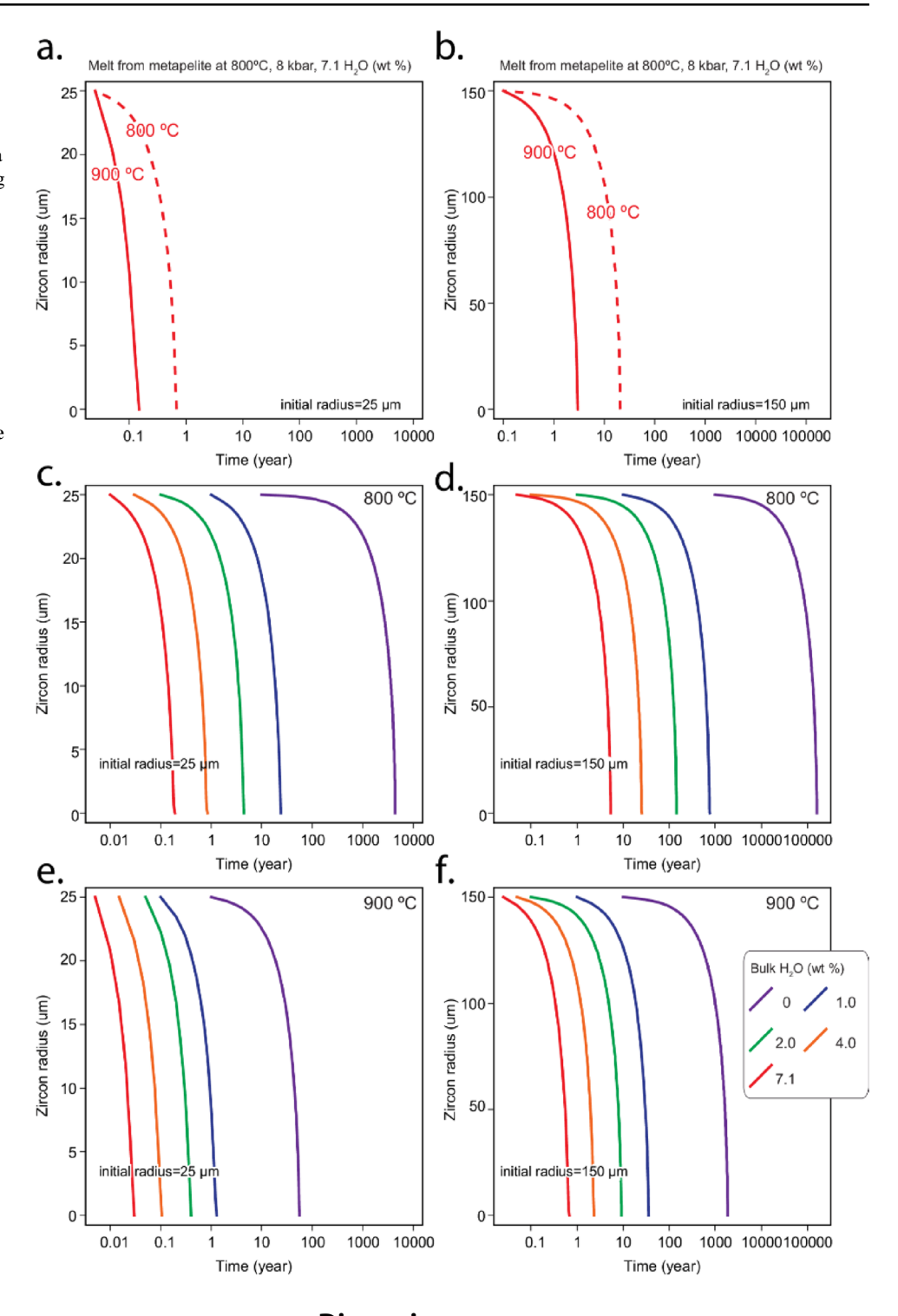
of Bindeman and Melnik (2016) which calculates the timescales of dissolution of spherical zircon grains in arbitrary melt compositions. We have carried out the calculations in a set of starting bulk compositions that include the measured bulk composition of the leucosome (CM 27B-17), the melt composition obtained in the pseudosection calculation, as well as a standard dacite and a rhyolite (Supplementary Information Tables 14 and 15).

The Zr concentrations in melt at zircon saturation are obtained from Gervasoni et al. (2016) and diffusion coefficients of Zr in melt were calculated using the model of Fanara et al. (2017) and the viscosity model of Giordano et al. (2008) (Supplementary Material Fig. 4). With these parameters, calculations were carried out for a range of water contents in melt (0-4.0 wt%) and temperatures (800-900 °C) for zircon crystals ranging in size from 25 to 150 µm (i.e. the range of sizes found in the pelite). Based on the observation that the leucosome forms outcrop scale bodies, the melt pool in contact with the zircons was taken to be infinite. We found that in most cases, the zircon crystals dissolve completely within a few thousand years (Fig. 8). Survival timescales increase dramatically as temperature and water contents drop, but even at the lowest water contents (dry melt) and temperature (800 °C), the largest zircon crystals survive only for 1,600,000 years, and even with a little bit of water in the melt these timescales drop to a few tens of thousands of years.

These results demonstrate that with the degree of melting experienced by the pelite, zircons from it are very unlikely to survive in the leucosome. Similar inferences could be drawn from the modeling studies of Kelsey et al. (2008) and Yakymchuk and Brown (2014) as well, but these authors assumed equilibrium in their calculations and therefore it is not possible to obtain information about timescales of residence from those studies we have obtained above. The results of our calculations explain why the REE patterns and the dates of zircon in the leucosome are so different from those found in the pelite. These results also help us to interpret the significance of the dates (and REE patterns) from the zircons in the leucosome. All zircons (group L1) would have had to crystallize from the melt during cooling. As can be seen from Fig. 8, a melt saturated with Zr at ~850 °C quickly becomes oversaturated during cooling and could precipitate zircon. Therefore, we interpret that the ages of these zircons belonging to group L1 effectively date the M2 event, or more precisely, the time of initial cooling just after the peak temperature was attained. As will be shown below, the REE patterns of the zircons are consistent with this interpretation. The zircon rims (Group P2 and Group L2) with different REE signatures and younger dates, would have formed in later events. Significantly for later tectonic interpretations, the results of the calculations establish that



Fig. 8 Zircon dissolution kinetics illustrated using radius of zircon grains vs. time plots. Model calculations used the method of Bindeman and Melnik (2016). The melt composition is one calculated for a metapelitic bulk composition using the Perple X software. Details are provided in Supplementary Information Table 14. Different panels show the effects of various sets of parameters: a initial radius 25 um. and **b** initial radius 150 µm, both at 800 °C with 7.1 wt% H₂O in the melt. c initial radius of 25 μm and d initial radius of 150 µm, both at 800 °C with variable water contents in the melt of 0-7.1 wt% e Same as c and d, respectively, but at 900 °C



the rocks could not have been at high temperatures between M3A and M3B events and a period of residence at low temperatures is necessary i.e. cooling between M3A and M3B could not have been monotonously continuous.

Discussion

Metamorphic evolution constrained by zircon and garnet geochronology

Sub-solidus growth of garnet and zircon: the M1 event

Reaction textures and phase equilibrium modelling have



79

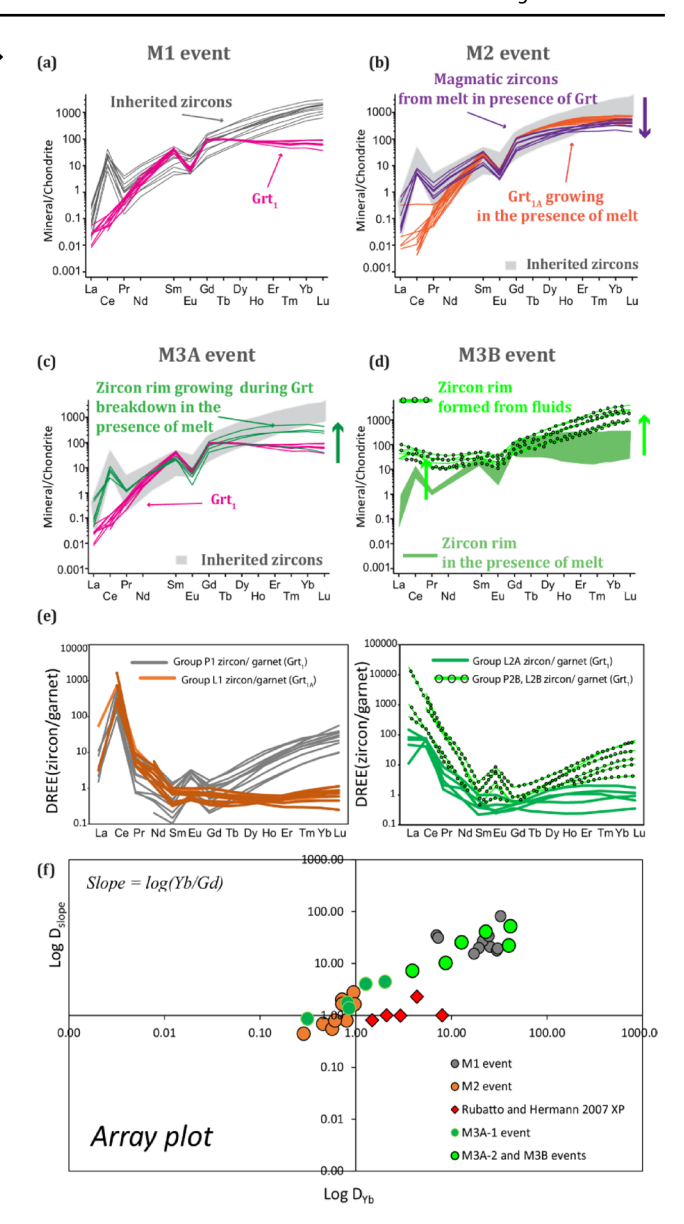
Fig. 9 Chondrite normalized diagrams of the REE composition of dated zircon and garnet. The arrows highlight relevant changes in REE between different growth. a, e and f REE patterns from detrital zircon (Group P1) and garnet (Grt₁) in the metapelite illustrate disequilibrium partitioning during garnet growth. Garnet exhibits flat REE profiles lacking HREE enrichment, contrasting with coexisting HREE-enriched zircons. This implies that REE partitioning between zircon and garnet did not reach equilibrium; b,e and f REE patterns of garnet from leucosome (Grt_{1A}) and zircon crystallized during the M2 metamorphic event (Group L1) indicate equilibrium partitioning from a melt. Grt_{1A}, a peritectic garnet distinct from earlier Grt₁, is enriched in HREE relative to Grt, but remains somewhat depleted due to coeval zircon growth from the same melt; c.e and f Zircon rims from both the leucosome and pelite (Group P2A and L2A) show moderate HREE enrichment, attributed to garnet breakdown during the M3 metamorphic event, when melt reacted with garnet to form biotite; d,e and f Late-stage zircon rims (Group P2B and L2B) with dark CL response exhibit LREE-enriched REE patterns and irregular morphologies, consistent with sub-solidus growth in the presence of fluids; e Traditional DREE plot showing relation of different events; f Array plot following Taylor et al. 2017 in which for comparison, Rubatto and Hermann 2007 experimental data is plotted. Chondrite normalisation values are from Sun and McDonough (1989)

shown that garnet in the metapelite (Grt₁) grew by the biotite dehydration reaction 1. During such sub-solidus growth at T~700 °C, pre-existing zircon in the metapelite (Group P1, date range: 3149-3535 Ma) would neither react nor exchange elements because of its refractory nature and slow diffusion rates of elements such as REE (e.g. Cherniak et al. 1997; Rubatto 2002). The REE patterns observed in the zircons and garnets in the rock appear to corroborate this behaviour (Fig. 9a, e,f). The HREE are enriched in zircon while the garnets do not show such an enrichment as they have a flat REE pattern that would not be in partitioning equilibrium with the zircon (e.g. using the partition coefficients of Rubatto and Hermann (2007).

The contrasting REE pattern has several consequences for the distribution of REE (as well as U, Th and Pb) in the rock: (i) Partitioning of HREE between zircon and garnet did not attain equilibrium. As a significant proportion of the HREE budget of the rock is likely to have been contained in zircon, the garnet grew with a somewhat depleted HREE content. (ii) The U-Pb dates from zircon likely represent the age of formation of the zircons, and (iii) Lu-Hf isotopes of garnet may not be able to provide well constrained garnetwhole rock dates, because the entire matrix (which includes the zircon grains) was not equilibrated with the garnet. For example, with ~1.4 ppm Lu in garnet and ~49 ppm in zircon, and a modal abundance of garnet of ~10%, even a small amount of zircon would contribute substantially to the bulk rock concentration of 0.2 ppm Lu.

Garnet and zircon evolution during melting: M2 event

During the M2 metamorphic event, the metapelite crosses the solidus as the temperature increases, likely accompanied



by burial, resulting in the formation of melt through the consumption of biotite by reaction 2. As the reaction progresses, Grt_{1A} in the melt grows as a possible peritectic phase. This Grt_{1A} is texturally and compositionally different from Grt₁ both in terms of major as well as trace elements. Zircons also crystallize from this melt during cooling from the peak temperature. The U-Pb analyses of zircons from the leucosome give an age range of formation of such magmatic zircons from 2989 to 3300 Ma. This inference is supported by the Ti-in-zircon thermometry, which gives a temperature range of 850-933 °C.

The calculated temperatures from the zircons in the leucosome fall well within the melt present field calculated by the phase equilibria modelling, and near the P-T region where biotite is almost exhausted, as observed in the rock. Note, however, that our modelling showed that at these conditions



most pre-existing zircon grains would be dissolved in the melt. As a result, the peritectic garnets and the zircons, both growing from the same melt (as well as dissolving and reprecipitating to attain textural equilibrium, facilitated by the presence of melt (Kelsey et al. 2008; Yakymchuk and Brown 2014), could attain partitioning equilibrium with each other. This is found to be the case (Fig. 9b, e,f), where Grt_{1A} is found to be much more enriched in HREE compared to Grt₁, but still somewhat depleted in HREE because of the coeval growth of zircon, another phase that sequesters HREE.

The HREE concentrations in the zircons and garnets in the leucosome are consistent with partitioning equilibrium relationship of these elements in the two phases (Rubatto and Hermann 2007). These observations constrain the age of melting and immediate subsequent cooling between 2989 and 3300 Ma. Note that this is consistent with the fact that the pre-existing (? detrital) zircons found in the metapelite (distinguished on the basis of their REE patterns) are mostly older (Fig. 5).

Garnet breakdown and zircon growth during cooling in the presence of melt: M3A event

The rims of the zircons (magmatic, in the leucosome, as well as the rims of older detrital zircons in the pelite) are characterized by a relative enrichment of HREE. We know from the petrological information (reaction textures and phase equilibrium modelling) that the M3A event is characterized by the back reaction of melt with garnet to form biotite at the expense of garnet. Thus, such breakdown of garnet would release HREE which is expected to be sequestered in zircon rims that may have been growing at the time. Growth of zircon is expected because as the melt crystallizes and back reacts, its volume decreases, leading to an enrichment of the incompatible element Zr in the residual melt and ultimately, its saturation (e.g. Bea et al. 2022 - even if that study relates to mafic melts, the principle is the same, as well as Kelsey et al. 2008 and Yakymchuk and Brown 2014).

The enrichment of HREE in these zircon rims is however, not as high as in the protolith detrital zircons (shown for comparison in grey in Fig. 9c, e,f) because a significant amount of garnet is still present in the rock. The dates of these zircons, ranging from 2626 to 3141 Ma provide some constraints on the timing of this event. It is important to note that the majority of the dates (40 out of 47) lie between 3141 – 2914 Ma for the metapelite. In the leucosome, out of a total range of dates from 2503 to 3081 Ma, six out of nine lie within 2990–3081 Ma with three isolated younger dates.

Metasomatic fluid induced sub-solidus zircon and garnet growth at lower temperatures: M3B event

The M3B stage is marked by sub-solidus growth of zircon rims (Group P2B, L2B) which are dark in the CL images. These zircon rims are irregularly formed and give scattered, different dates, but all younger than the above, such as 2503 ± 19 and 2630 ± 56 Ma. The chondrite normalized REE pattern of these zircon rims are also LREE enriched as compared to HREE. The relatively higher LREE in the REE patterns of these zircons (Fig. 9d, e,f) as well as textural attributes suggest growth in the presence of fluids (metasomatic, hydrothermal etc.). These attributes, as well as the younger end of the age spectrum, coincide with the formation of Grt_2 in the associated mafic rocks. Recall that Grt_2 also has a REE pattern that indicates hydrothermal (high temperature fluid) activity, and a Lu-Hf date of 2450 ± 66 Ma (Basak et al. 2023).

The studies of the metabasic rocks from the region showed that metamorphism between $\sim 2700-3100$ Ma was followed by residence of the rocks/crustal segment at relatively low temperatures (< 500 °C, i.e. temperatures below which diffusive modification of garnet is considered to be negligible) for $\sim 100 \, \mathrm{s}$ of million years before a second event accompanied by metasomatic/hydrothermal (high temperature fluid) activity occurred at ~ 2400 Ma (Basak et al. 2023). These results are consistent with and are corroborated by this study of the metapelitic rocks.

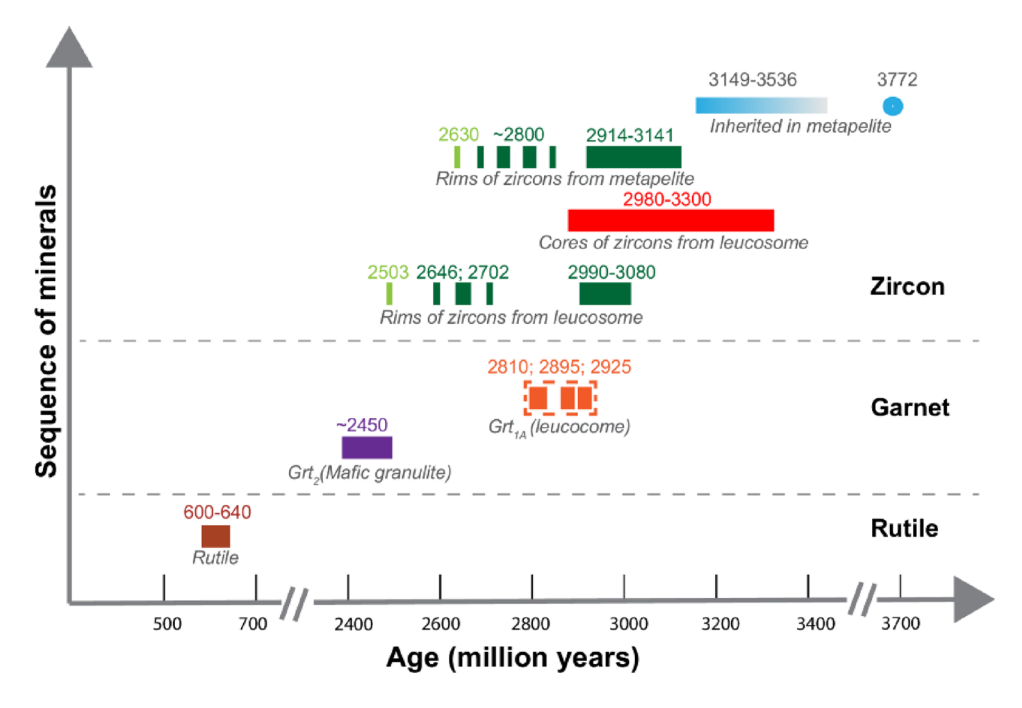
As shown above, the rocks remained above the solidus curve between 2700 and 3300 Ma, permitting a relatively long residence time, at least in pulses, in a melt present field. This was followed by residence at lower temperatures for an extended period, with intermittent metasomatic/hydrothermal (high temperature fluid) activity, which appears to have climaxed to a major metamorphic reaction event (e.g. formation of Grt_2 in the metabasites) at ~2400 Ma. This is followed by the M4 event of biotite formation along rims of garnet, timing of which is uncertain.

The rutile dates of 600–640 Ma corresponding to **M5** event point to some activity at moderately high temperatures near pan-African times - in the intervening period the rocks may have been exhumed to the surface and re-buried or have been exhumed to only shallower levels within the crust.

Figure 10 summarizes the geochronological information from the zircon as well as Grt_{1A} (leucosomes) and Grt₂ (metabasic rock). Overall, the data reveals (a) long lasting high temperature metamorphic events and (b) long residence times at low temperatures in between these events, (c) and occurrence of events at multiple times between 2700 and 3300 Ma and again between 2600–2400 Ma, and later between 610 and 640 Ma (Fig. 11).



Fig. 10 Summary of ²⁰⁷Pb/²⁰⁶Pb dates of zircons and rutile and ¹⁷⁶Lu-¹⁷⁶Hf ages of garnet from different samples. See text for details



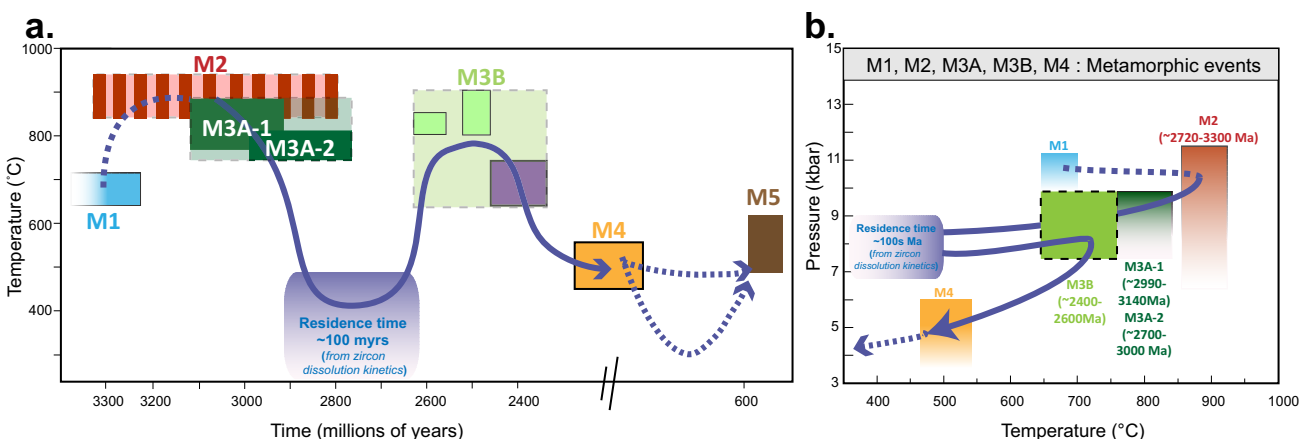


Fig. 11 The inferred pulsed a T-t path and b P-T path followed by the pelitic rock and leucosome. M1 event (blue box): Based on phase diagram modeling. M2 event (red box): Based on Ti in zircon thermometry, U-Pb dates of relevant zones (usually cores) of zircons identified by trace element patterns and Lu-Hf garnet geochronology. The striped pattern hints at discrete ages recorded in the zircons and garnets, rather than a continuum, within the given temporal range. M3A-1 event (dark green box): Based on Ti in zircon thermometry, U-Pb dates of zircon rims. M3A-2 event (dark green box): Based on Ti in zircon thermometry, U-Pb dates of zircon rims. The distinction between M3A-1 and M3A-2 is based on differences in REE patterns. M3B event (pale green

Comparison with previous studies and geodynamic and regional implications

The dates of zircon found in this study agree well with those obtained by Amaldev et al. (2016) from rocks from the same region. They interpreted the precursors of the metapelite to be volcano-sedimentary trench sequences with an age range of 3248–3506 Ma, which is comparable

box): Much younger zircon rims with REE patterns similar to M3A-2 and well-constrained P-T-t (purple box) from adjacent mafic rocks (Basak et al. 2023). M4 event (golden box): Based on Fe-Mg exchange thermometry with garnet-rim and biotite; timing is uncertain. M5 event (brown box): Based on dates from rutile and U-Pb closure temperature of rutile [490–640 °C (Cherniak 2000)], along with the constrain that heating was not high enough to affect/reset garnet and zircon ages. Please note that the P-T region of M3A-M3B is approached once during cooling and once during heating (panels a, b) and that the path between M4 and M5 is uncertain, as indicated by two possible alternatives shown as dashed lines. See text for details

to the dates obtained by us from the cores of zircons in the metapelite (3149–3535 Ma). Furthermore, Amaldev et al. (2016) interpreted the upper intercept age of 3080 ± 35 Ma (MSWD=2.3) defined by zircon analyses along a Discordia line to be the age of a metamorphic overprint. This age is comparable to the ~2990–3080 Ma age of metamorphism inferred from our study of petrological reactions correlated with concordant age determinations from the zircon rims. Yu



et al. (2021) studied a range of lithologies (mafic granulite, charnockite, metapelites and fuchsite quartzite) in neighbouring regions obtaining results similar to ours. Zircon and monazite U-Pb dating indicate detrital zircon ages up to ~3.5 Ga, with metamorphic overgrowths and monazite ages of 3.1-3.0 Ga, and later thermal overprinting at 2.8–2.6 Ga (Yu et al. 2021). They also show that zircons exhibit distinct core-rim textures with darker magmatic cores and lighter metamorphic rims that were identified through isotopic signature and variation in REE patterns. The magmatic cores were found to be enriched in HREE whereas the rims have a flat HREE pattern from all the rock types (Yu et al. 2021).

Amaldev et al. (2016) also measured zircon Hf-isotopes and found that the zircon cores of the metapelite, which they interpreted to be magmatic, were derived mostly from reworked Eoarchean crustal materials with sources as old as ~ 3.8 Ga. Materials with the source age of up to ~ 3.8 Ga is consistent with the single data point that yields~3.7 Ga from our metapelite, although most of the grains are much younger, possibly pointing to a relatively younger source. This would be consistent with the observation of Amaldev et al. (2016) that the associated magmatic rocks in the region have a considerable juvenile Mesoarchean component. It is also worth noting that they found rocks with kyanite in a neighbouring region, which adds support to our earlier conjecture that the absence of kyanite in our samples, even though the inferred P-T paths go through fields where kyanite should be stable, could be related to metastable lack of crystallization of kyanite.

Notwithstanding all the agreements, there remains an unresolved controversy for this region that has important implications for palaeo reconstructions. While some studies (e.g. Ishwar- Kumar et al. (2013); Rekha et al. (2014) correlated the Mercara shear zone with the $\sim\!2.4$ Ga Betsimisaraka suture zone in east-central Madagascar, Amaldev et al. (2016) found evidence for metamorphism at $\sim\!3.0$ Ga, which they interpreted as the time when the Coorg block joined the Dharwar block.

In this present study we find that the major metamorphic event (e.g. melting) occurred over an extended period between 2700 and 3300 Ma, followed by partial cooling and residence at mid crustal depths, where metasomatic/hydrothermal (high temperature) fluid activities possibly caused repeated but occasional dissolution-reprecipitation of zircons between 2900 and 3080 Ma. Subsequently, between 2400 and 2600 Ma, a heating event (this study and Basak et al. 2023) accompanied by high temperature metasomatic/hydrothermal activity led to the formation of metamorphic minerals such as garnets (grossular-rich) in mafic bulk compositions or LREE enriched zircon rims in the metapelite and the leucosome. A similar P-T-t history has been reported

in Archean granulite terrane of the North China Craton (Wang et al. 2023).

In our study, as the peak temperature of the second heating event did not exceed the peak metamorphic conditions of the previous metamorphism, the signature of this event is only subtle and can only be properly resolved when high resolution information on timescales are available. Geospeedometry on the mafic mineral assemblages (Basak et al. 2023) was particularly useful for this - the results from the pelitic bulk composition helps to corroborate the history and provide details for the higher temperature end of the P-T path. Thus, in a regional context, the interpretation of the two events may be the amalgamation of the Coorg block with the Dharwar block between 2990 and 3300 Ma, followed by activity on an equivalent of the Betsimisaraka suture zone in east-central Madagascar between 2400 and 2600 Ma. Even after the second event, it is not clear that the rocks were exhumed totally and then affected by metamorphism again. It is quite possible that they were partially exhumed and resided at cooler upper-mid crustal levels, where the previous records were not disturbed and reset, to undergo a final metamorphic event at lower temperatures yet between 600 and 640 Ma. The temperatures of this event would have been high enough to reset dates in rutile, but not in phases such as garnet or zircon. The final exhumation may have occurred only after that latest event, recording a multistage thermal history spanning several hundred million years where each metamorphic event consisted of thermal pulses of shorter durations.

If only geochronological data were used, it may have been tempting to connect all the dots (T-t points determined using closure temperature concepts) inferring a continuous evolution, but that would point to extremely long residence times at relatively high temperatures. That would not be consistent with the survival of zircons in molten systems. This study reveals the importance of considering the petrological reaction history in conjunction with timescale data (geochronology in this study, kinetics of zircon dissolution, geochronology and geospeedometry from Basak et al. 2023) to identify multistage or pulsed thermal evolutions (e.g. Bhowmik and Chakraborty 2017; Dasgupta et al. 2022).

The long residence time inferred in the melt-present P-T field also provides insights into the geodynamic processes that may have been responsible for the metamorphism. It is difficult to sustain temperatures on the order of 800 °C for 100's of millions of years in a modern-day plate tectonic setting (e.g. see Faccenda et al. 2008). However, early styles of plate tectonics on a hotter Earth open the possibility of exactly such long lasting events through the process of peelback that dominates under hotter conditions (Chowdhury et al. 2017, 2020). Long lasting events can occur in such settings because the process of peel back of a colliding slab



allows hot asthenospheric mantle to upwell and provide a continuous supply of heat that sustains the high temperatures in the overlying crustal regions for long times. The long residence time of the rocks in melt-present field, as found in this study, points to the operation of such tectonics between 2990 and 3300 Ga in the Coorg-Dharwar region. The same inference has been made using other lines of evidence in Basak et al. 2023 in their study of metabasites from the same region. Together, these studies provide strong evidence in support of operation of the peel-back form of early plate tectonics by 3.0 Ga in the Earth's history.

Conclusion

This study of the records of high temperature evolution of a metapelite from the vicinity of the Mercara Shear zone in the Archean terrain of Coorg (S. India) revealed a multistage evolution along an overall clockwise P-T path that was however, not monotonous - residence of the lithological packet at adjacent P-T coordinates was intervened by sojourns at lower temperatures. A newly developed tool of modeling the kinetics of dissolution of zircon in conjunction with zircon ages and trace element signatures to associate the ages to specific metamorphic reactions at given P-T conditions enables the recognition of such non-monotonous evolution. Thus, a given P-T coordinate during the evolution of the rock was approached from different directions (e.g. prograde vs. retrograde) at different events during the evolution of the rock (Fig. 11). This recognition may help to reconcile debates related to the tectonic reconstructions in the region (e.g. whether amalgamation of Dharwar and Coorg cratons or activity along an equivalent of the Betsimisaraka suture zone in east-central Madagascar is recorded in these rocks). Further, the long (several 100 million years) duration of residence at relatively high (~800 °C) temperatures is consistent with the operation of peel back style early plate tectonics (Chowdhury et al. 2017) in the region during the late Archean.

Supplementary **Information** The online version contains supplementary material available at https://doi.org/10.1007/s00410-0 25-02263-z.

Acknowledgements We are thankful to Dr. Jasper Berndt of University of Münster, Germany for supporting with the in-situ LA-ICPMS measurements, and Dr. Niels Jöns, Dr. Thomas Fockenberg, Kirsten Keppler and Ute Gundert at the Ruhr University Bochum, Germany for supporting with electron microprobe and XRF analyses. We are also grateful to Dr. Eric Hasenstab and Dr. Jonas Tusch at the University of Cologne for their assistance in the Lu-Hf measurements and Dr. Richard Albert Ropert for his valuable assistance in the zircon U-Pb and trace element measurements at FIERCE, Goethe-University Frankfurt. This is FIERCE contribution 207. Last but not the least we are grateful to Prof. Ravindra Kumar for assisting in the field trip

and insightful discussions on this topic. We acknowledge reviews from Prof. Chris Clark, Dr. John Pownall and an anonymous reviewer. Meticulous review with attention to detail from the handling editor Prof. Daniela Rubatto and Prof. Dante Canil significantly improved the presentation of results in this manuscript.

Funding Open access funding provided by Copenhagen University. This work was supported by DFG Schwerpunktprogramm 1833 "Building a Habitable Earth" (DFG project number: CH 166/17-1), the young researcher mobility grant that was awarded to Dr. Sampriti Basak to carry out all the analytical works in Bochum, Münster, Cologne and Frankfurt, Germany and the scholarship award from Wilhelm and Günter Esser Foundation WS2019/20, Germany (RUB Research School) awarded to Dr. Sampriti Basak.

Open Access This article is licensed under a Creative Commons Attribution 4.0 International License, which permits use, sharing, adaptation, distribution and reproduction in any medium or format, as long as you give appropriate credit to the original author(s) and the source, provide a link to the Creative Commons licence, and indicate if changes were made. The images or other third party material in this article are included in the article's Creative Commons licence, unless indicated otherwise in a credit line to the material. If material is not included in the article's Creative Commons licence and your intended use is not permitted by statutory regulation or exceeds the permitted use, you will need to obtain permission directly from the copyright holder. To view a copy of this licence, visit http://creativecommons.o rg/licenses/bv/4.0/.

References

Amaldev T, Santosh M, Tang L, Baiju KR, Tsunogae T, Satyanarayanan M (2016) Mesoarchean convergent margin processes and crustal evolution: petrologic, geochemical and Zircon U-Pb and Lu-Hf data from the Mercara suture zone, Southern India. Gondwana Res 37:182–204. https://doi.org/10.1016/j.gr.2016.05.017

Basak S, Hasenstab E, Bhowmik SK, Gerdes A, Dasgupta S, Münker C, Kumar GR, Chakraborty S (2023) Thermal and chemical evolution of an archean collision zone: insights from P-T-t history of mafic granulites from the Coorg block, S. India. J Petrol 64(5):egad026. https://doi.org/10.1093/petrology/egad026

Bea F, Bortnikov N, Cambeses A, Chakraborty S, Molina JF, Montero P, Morales I, Silantiev S, Zinger T (2022) Zircon crystallization in low Zr mafic magmas: possible or impossible? Chem Geol 602:120898. https://doi.org/10.1016/j.chemgeo.2022.120898

Bhowmik SK, Chakraborty S (2017) Sequential kinetic modelling: a new tool decodes pulsed tectonic patterns in early hot orogens of Earth. Earth Planet Sci Lett 460:171-179. https://doi.org/10.101 6/j.epsl.2016.12.018

Bindeman IN, Melnik OE (2016) Zircon survival, rebirth and recycling during crustal melting, magma crystallization, and mixing based on numerical modelling. J Petrol 57(3):437-460. https://do i.org/10.1093/petrology/egw013

Breton J, Thompson AB (1988) Fluid-absent (dehydration) melting of biotite in metapelites in the early stages of crustal anatexis. Contrib Miner Petrol 99(2):226–237. https://doi.org/10.1007/BF

Cawood PA, Hawkesworth CJ, Dhuime B (2022) The continental record and the generation of continental crust. Geol Soc London Speci Publ 389: 1-22. https://doi.org/10.1130/B30722.1

Cherniak DJ (2000) Pb diffusion in rutile. Contrib Mineral Petrol 139(2):198-207. https://doi.org/10.1007/PL00007671



- Cherniak DJ, Hanchar JM, Watson EB (1997) Diffusion of tetravalent cations in zircon. Contrib Mineral Petrol 127(4):383–390. https://doi.org/10.1007/s004100050287
- Chetty TRK, Mohanty DP, Yellappa T (2012) Mapping of shear zones in the Western Ghats, southwestern part of Dharwar craton. J Geol Soc India 79(2):151–154. https://doi.org/10.1007/s12594-012-0023-1
- Chowdhury P, Gerya T, Chakraborty S (2017) Emergence of silicic continents as the lower crust peels off on a hot plate-tectonic Earth. Nat Geosci 10(9):698–703. https://doi.org/10.1038/ngeo 3010
- Chowdhury P, Chakraborty S, Gerya TV, Cawood PA, Capitanio FA (2020) Peel-back controlled lithospheric convergence explains the secular transitions in archean metamorphism and magmatism. Earth Planet Sci Lett 538:116224. https://doi.org/10.1016/j.epsl. 2020.116224
- Connolly JAD (2005) Computation of phase equilibria by linear programming: a tool for geodynamic modeling and its application to subduction zone decarbonation. Earth Planet Sci Lett 236:524–541. https://doi.org/10.1016/j.epsl.2005.04.033
- Dasgupta S, Chakraborty S, Neogi S (2009) Petrology of an inverted Barrovian sequence of metapelites in Sikkim Himalaya, India: constraints on the tectonics of inversion. Am J Sci 309(1):43–84. https://doi.org/10.2475/01.2009.02
- Dasgupta A, Bhowmik SK, Dasgupta S (2022) Transition in thermal history and recurring burial-exhumation cycles along colder thermal gradients at the Archaean-Proterozoic boundary: new insights from the Western Dharwar craton, South India. J Petrol 63(6):egac041. https://doi.org/10.1093/petrology/egac041
- Eckert JO, Newton RC, Kleppa OJ (1991) The ΔH of reaction and recalibration of garnet-pyroxene-plagioclase-quartz geobarometers in the CMAS system by solution calorimetry. Am Mineral 76(1–2):148–160
- Faccenda M, Gerya TV, Chakraborty S (2008) Styles of post-sub-duction collisional orogeny: influence of convergence velocity, crustal rheology and radiogenic heat production. Lithos 103(1):257–287. https://doi.org/10.1016/j.lithos.2007.09.009
- Fanara S, Sengupta P, Becker HW, Rogalla D, Chakraborty S (2017) Diffusion across the glass transition in silicate melts: systematic correlations, new experimental data for Sr and Ba in calcium-aluminosilicate glasses and general mechanisms of ionic transport. J Non-cryst Solids 455:6–16. https://doi.org/10.1016/j.jnoncryso 1.2016.10.013
- Ferry JM, Spear FS (1978) Experimental calibration of the partitioning of Fe and Mg between biotite and garnet. Contrib Mineral Petrol 66(2):113–117. https://doi.org/10.1007/BF00372150
- Ferry J, Watson E (2007) New thermodynamic models and revised calibrations for the Ti-in-zircon and Zr-in-rutile thermometers. Contrib Mineral Petrol 154(4):429–437. https://doi.org/10.1007/s00410-007-0201-0
- Furley C, Lindeman JR (1988) Experimental melting relationships in the system NaAlSi₃O₈–KAlSi₃O₈–SiO₂–H₂O and implications for the generation of granitic magmas. J Petrol 29:1257–1283
- Ganguly J, Cheng W, Tirone M (1996) Thermodynamics of aluminosilicate garnet solid solution: new experimental data, an optimized model, and thermometric applications. Contrib Mineral Petrol 126(1):137–151. https://doi.org/10.1007/s004100050240
- Gerdes A, Zeh A (2006) Combined U–Pb and hf isotope LA-(MC-) ICP-MS analyses of detrital zircons: comparison with SHRIMP and new constraints for the provenance and age of an Armorican metasediment in central Germany. Earth Planet Sci Lett 249(1):47–61. https://doi.org/10.1016/j.epsl.2006.06.039
- Gerdes A, Zeh A (2009) Zircon formation versus Zircon alteration New insights from combined U-Pb and Lu-Hf in-situ LA-ICP-MS analyses, and consequences for the interpretation of archean

- Zircon from the central zone of the Limpopo belt. Chem Geol 261(3):230–243. https://doi.org/10.1016/j.chemgeo.2008.03.005
- Gervasoni F, Klemme S, Rocha-Júnior ER, Berndt J (2016) Zircon saturation in silicate melts: a new and improved model for aluminous and alkaline melts. Contrib Mineral Petrol 171(3):21. https://doi.org/10.1007/s00410-016-1227-y
- Giordano D, Russell JK, Dingwell DB (2008) Viscosity of magmatic liquids: a model. Earth Planet Sci Lett 271(1–4):123–134. https://doi.org/10.1016/j.epsl.2008.03.038
- Griffin WL, Powell WJ, Pearson NJ, O'reilly SY (2008) Appendix A2: Glitter: data reduction software for laser ablation ICP–MS. https://doi.org/10.3749/9780921294801.app02
- Hasenstab E, Tusch J, Schnabel C, Marien CS, Van Kranendonk MJ, Smithies H, Howard H, Maier WD, Münker C (2021) Evolution of the early to late Archean mantle from Hf-Nd-Ce isotope systematics in basalts and komatiites from the Pilbara craton. Earth Planet Sci Lett 553:116627. https://doi.org/10.1016/j.epsl.2020. 116627
- Holland TJB, Powell R (2011) An improved and extended internally consistent thermodynamic dataset for phases of petrological interest, involving a new equation of state for solids. J Metamorph Geol 29:333–383. https://doi.org/10.1111/j.1525-1314.20 10.00923.x
- Hoskin PWO (2005) Trace-element composition of hydrothermal zircon and the alteration of Hadean zircon from the Jack hills, Australia. Geochim Cosmochim Acta 69(3):637–648. https://doi.org/10.1016/j.gca.2004.07.006
- Ishwar-Kumar C, Windley BF, Horie K, Kato T, Hokada T, Itaya T, Yagi K, Gouzu C, Sajeev K (2013) A rodinian suture in Western India: new insights on India-Madagascar correlations. Precambrian Res 236:227–251. https://doi.org/10.1016/j.precamres.2013.07.023
- Jochum KP, Willbold M, Raczek I, Stoll B, Herwig K (2005) MPI-DING reference glasses for in situ microanalysis: new reference values for element concentrations and isotope ratios. Geochem Geophys Geosyst 6:Q02004. https://doi.org/10.1029/2005GC00 1060
- Kelsey DE, Hand M, Clark C (2008) Thermobarometric modelling of zircon and monazite growth in melt-bearing systems: examples using model metapelitic and metapsammitic granulites. J Metamorph Geol 26:199–212. https://doi.org/10.1111/j.1525-1314.20 07.00757.x
- Kretz R (1983) Symbols for rock-forming minerals. Am Mineral 68:277-279
- Ludwig KR (2001) Isoplot/Ex version 2.49: a geochronology toolkit for Microsoft Excel. Berkeley Geochronol Center Spec Publ 55(1): 49
- Münker C, Weyer S, Scherer E, Mezger K (2001) Separation of high field strength elements (Nb, Ta, Zr, Hf) and Lu from rock samples for MC ICPMS measurements. Geochem Geophys Geosyst. http s://doi.org/10.1029/2001GC000183
- Patiño Douce AE, Beard JS (1995) Dehydration-melting of biotite gneiss and quartz amphibolite from 3 to 15 Kbar. J Petrol 36:707-738
- Rekha S, Bhattacharya A, Chatterjee N (2014) Tectonic restoration of the precambrian crystalline rocks along the West Coast of India: correlation with Eastern Madagascar in East Gondwana. Precambrian Res 252:191–208. https://doi.org/10.1016/j.precamres.201 4.07.013
- Roduit N (2025) JMicroVision: Image analysis toolbox for measuring and quantifying components of highdefinition images. Version 1.3.5. https://jmicrovision.github.io. Accessed Apr 2025
- Rubatto D (2002) Zircon trace element geochemistry: partitioning with Garnet and the link between U–Pb ages and metamorphism. Chem Geol 184(1):123–138. https://doi.org/10.1016/S0009-254 1(01)00355-2



- Rubatto D, Hermann J (2007) Experimental zircon/melt and zircon/ garnet trace element partitioning and implications for the geochronology of crustal rocks. Chem Geol 241(1):38-61. https://do i.org/10.1016/j.chemgeo.2007.01.027
- Santos MM, Lana C, Scholz R, Buick I, Schmitz MD, Kamo SL, Gerdes A, Corfu F, Tapster S, Lancaster P, Storey CD, Basei MAS, Tohver E, Alkmim A, Nalini H, Krambrock K, Fantini C, Wiedenbeck M (2017) A new appraisal of Sri Lankan BB zircon as a reference material for LA-ICP-MS U-Pb geochronology and Lu-Hf isotope tracing. Geostand Geoanal Res 41:335–358. https: //doi.org/10.1111/ggr.12167
- Santosh M, Yang QY, Ram Mohan M, Tsunogae T, Shaji E, Satyanarayanan M (2014) Cryogenian alkaline magmatism in the Southern granulite terrane, India: petrology, geochemistry, Zircon U-Pb ages and Lu-Hf isotopes. Lithos 208-209:430-445. https://doi.or g/10.1016/j.lithos.2014.09.016
- Scherer E, Münker C, Mezger K (2001) Calibration of the lutetiumhafnium clock. Science 293(5530):683-687. https://doi.org/10.1 126/science.1061372
- Sláma J, Košler J, Condon DJ, Crowley JL, Gerdes A, Hanchar JM, Horstwood MSA, Morris GA, Nasdala L, Norberg N, Schaltegger U, Schoene B, Tubrett MN, Whitehouse MJ (2008) Plesovice zircon – a new natural reference material for U–Pb and hf isotopic microanalysis. Chem Geol 249:1-35
- Söderlund U, Patchett PJ, Vervoort JD, Isachsen CE (2004) The 176Lu decay constant determined by Lu-Hf and U-Pb isotope systematics of precambrian mafic intrusions. Earth Planet Sci Lett 219(3):311-324. https://doi.org/10.1016/S0012-821X(04)0001 2 - 3
- Sorcar N, Hoppe U, Dasgupta S, Chakraborty S (2014) High-temperature cooling histories of migmatites from the high Himalayan crystallines in Sikkim, India: rapid cooling unrelated to exhumation? Contrib Mineral Petrol 167(2):957. https://doi.org/10.1007 /s00410-013-0957-3
- Spear FS (2004) Fast cooling and exhumation of the Valhalla metamorphic core complex, southeastern British Columbia. Int Geol Rev 46(3):193–209. https://doi.org/10.2747/0020-6814.46.3.193
- Spear FS, Markussen JC (1997) Mineral zoning, P-T-X-M phase relations, and metamorphic evolution of some adirondack granulites, New York. J Petrol 38(6):757-783. https://doi.org/10.1093 /petroj/38.6.757
- Stacey JS, Kramers JD (1975) Approximation of terrestrial lead isotope evolution by a two-stage model. Earth Planet Sci Lett 26:207-221
- Sun Ss, McDonough WF (1989) Chemical and isotopic systematics of oceanic basalts: implications for mantle composition and processes. Geol Soc London Spec Publ 42(1):313-345. https://doi.or g/10.1144/GSL.SP.1989.042.01.19

- Sunil PS, Radhakrishna M, Kurian PJ, Murty BVS, Subrahmanyam C, Nambiar CG, Arts KP, Arun SK, Mohan SK (2010) Crustal structure of the western part of the Southern granulite terrain of Indian Peninsular shield derived from gravity data. J Asian Earth Sci 39(6):551–564. https://doi.org/10.1016/j.jseaes.2010.04.028
- Taylor RJM, Clark C, Harley SL, Kylander-Clark ARC, Hacker BR, Kinny PD (2017) Interpreting granulite facies events through rare earth element partitioning arrays. J Metamorph Geol 35(7):759-775. https://doi.org/10.1111/jmg.12254
- Van Kranendonk MJ, Kirkland CL, Cliff JB (2018) Oxygen isotopes and hafnium in Zircon record the evolution of the Archaean crust-mantle system. Nat Geosci 11:139-143
- Wang D, Mitchell RN, Guo J, Liu F (2023) Exhumation of an archean granulite terrane by paleoproterozoic orogenesis: evidence from the North China craton. J Petrol 64(6):egad035. https://doi.org/10 .1093/petrology/egad035
- White RW, Powell R, Holland TJB, Worley BA (2000) The effect of TiO₂ and Fe₂O₃ on metapelitic assemblages at greenschist and amphibolite facies conditions: mineral equilibria calculations in the system K₂O-FeO-MgO-Al₂O₃-SiO₂-H₂O-TiO₂-Fe₂O₃. J Metamorph Geol 18(5):497–511. https://doi.org/10.1046/j.152 5-1314.2000.00269.x
- White RW, Powell R, Holland TJB, Johnson TE, Green ECR (2014) New mineral activity-composition relations for thermodynamic calculations in metapelitic systems. J Metamorph Geol 32(3):261-286. https://doi.org/10.1111/jmg.12071
- Wiedenbeck M, Allé P, Corfu F, Griffin WL, Meier M, Oberli F, von Quadt A, Roddick JC, Spiegel W (1995) Three natural Zircon standards for U-Th-Pb, Lu-Hf, trace element and REE analyses. Geostand Newsl 19:1-23. https://doi.org/10.1111/j.1751-908X.1 995.tb00147.x
- Yakymchuk C, Brown M (2014) Behaviour of Zircon and monazite during crustal melting. J Geochem Explor 148:4–20. https://doi.o rg/10.1144/jgs2013-115
- Yu B, Santosh M, Amaldev T, Palin RM (2021) Mesoarchean (ultra)high temperature and high-pressure metamorphism along a microblock suture: evidence from earth's oldest khondalites in Southern India. Gondwana Res 91:129-151. https://doi.org/10.1 016/j.gr.2020.12.015
- Zhao L, Chakraborty S (2024) Kinetic controls on the thermometry of mantle rocks: a case study from the Xigaze ophiolites, Tibet. EMU Notes Mineral 21:189-222

Publisher's Note Springer Nature remains neutral with regard to jurisdictional claims in published maps and institutional affiliations.

